PENSOFT

SENCKENBERG
world of biodiversity

Leibniz Association

Phylogeny and evolution of large body size in the rove beetle genus *Phlaeopterus* Motschulsky, 1853 (Coleoptera: Staphylinidae: Omaliinae: Anthophagini)

Derek S. Sikes[1], Logan J. Mullen[1]

1 *University of Alaska Museum, University of Alaska Fairbanks, Fairbanks, AK, USA; Derek S. Sikes [dssikes@alaska.edu]*

http://zoobank.org/B392BC50-2DD6-442A-A75A-76D26555F2A9

Corresponding author: Derek S. Sikes (dssikes@alaska.edu)

Received 29 December 2020
Accepted 18 February 2021
Published 13 March 2021

Academic Editors Martin Fikacek, Klaus-Dieter Klass

Citation: Sikes DS, Mullen LL (2021) Phylogeny and evolution of large body size in the rove beetle genus *Phlaeopterus* Motschulsky, 1853 (Coleoptera: Staphylinidae: Omaliinae: Anthophagini). Arthropod Systematics & Phylogeny 79: 75–98. https://doi.org/10.3897/asp.79.e62554

Abstract

The omaliine rove beetle genus *Phlaeopterus* Motschulsky, 1853 contains 22 species. The genus is distributed across northwestern North America and eastern Asia. These beetles occur primarily along the edges of alpine snowfields and streams, habitats that are particularly sensitive to the impacts of climate change. Two species have not been collected since 1979 and 1984, one of which, *Phlaeopterus bakerensis* Mullen and Campbell, 2018, is a contender for the largest-bodied species among the over 1,600 species of the subfamily Omaliinae. Here, we present the first phylogeny of the genus, using Bayesian and maximum likelihood analyses based on DNA sequences from the mitochondrial gene COI and morphological data. We tested previous taxonomic hypotheses and most were rejected by all three analyses. *Phlaeopterus castaneus* Casey, 1893 is non-monophyletic based on COI sequences and may have hybridized with *P. loganensis* Hatch, 1957. We found support for the monophyly of the genus *Phlaeopterus*. Our analyses suggest the common ancestor of the genus had small-bodied adults (maximum body size under 5 mm) with ocelli. Within this small-bodied radiation of species, ocelli were lost once and there were two separate evolutionary transitions to large-bodied adults. Although all the large-bodied species are snowfield-associated and only 25% of the small-bodied species are, we did not find statistical support for a relationship between large body size and use of snowfield habitats. These findings represent the first modern phylogenetic reconstruction of species-level relationships within the rove beetle subfamily Omaliinae using both morphological and molecular data.

Keywords

Phlaeopterus, rove beetle, Staphylinidae, *Vellica*, *Lesteva*, *Unamis*, maximum likelihood, Bayesian, DNA barcoding

1. Introduction

The rove beetle subfamily Omaliinae contains more than 1,600 species in six tribes and 117 genera (Thayer 2016; Shavrin and Yamamoto 2019; A.F. Newton unpublished database 17 Jan. 2019). Omaliine body sizes have not been summarized for the world, but the vast majority of omaliine species have maximum adult body lengths less than 8 mm (M. Thayer in litt.). European Omaliinae are reported to have body sizes ranging from 1.7–7.0 mm (Za-

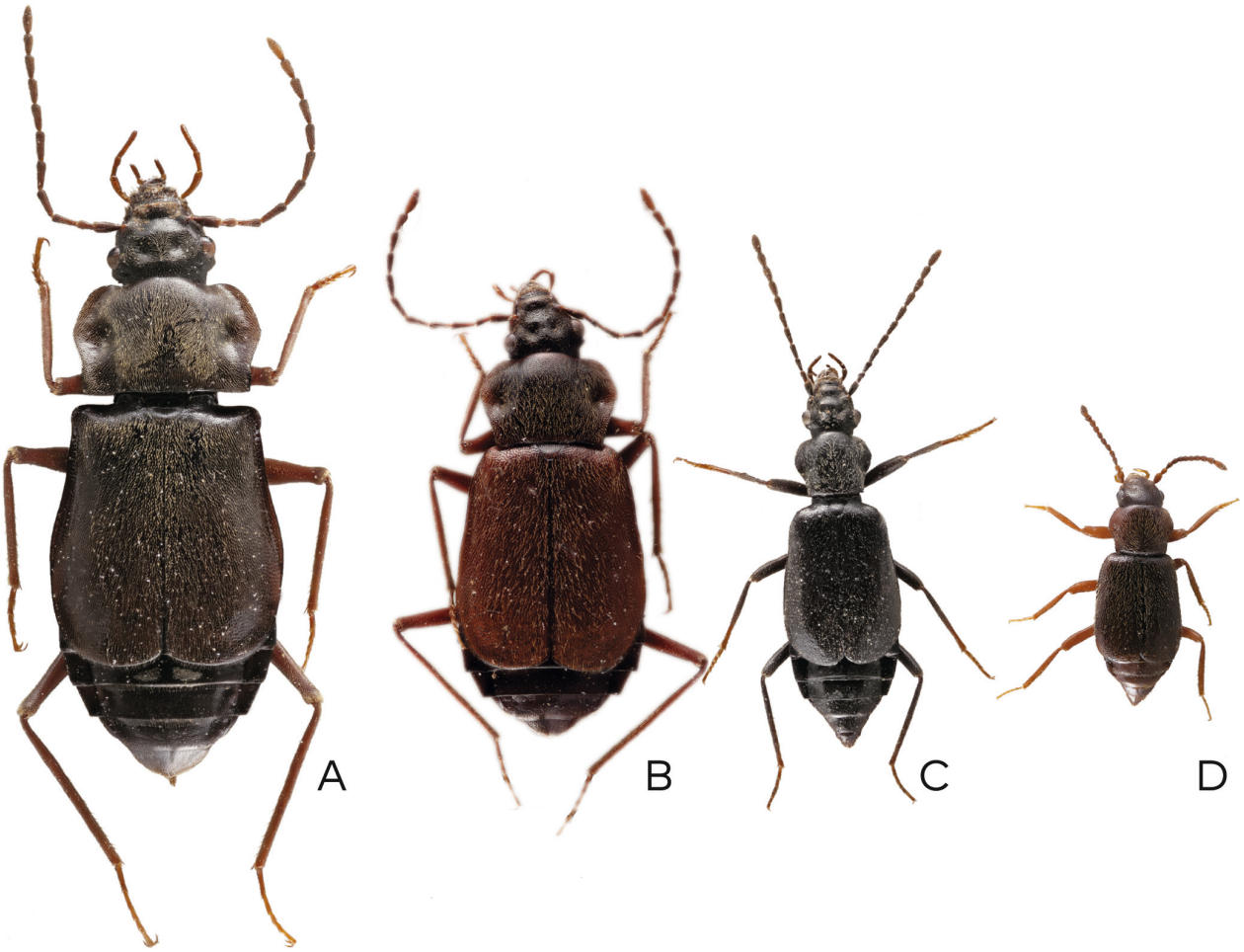

Figure 1. *Phlaeopterus* species size variation. A) *Phlaeopterus bakerensis*, the largest species: maximum length ~ 10 mm; B) *Phlaeopterus kavanaughi*, a large, wide bodied species, maximum length ~ 7.6 mm; C) *Phlaeopterus elongatus*, a large, elongate species, maximum length ~ 6.4 mm, and D) *Phlaeopterus obsoletus*, one of the smallest species: maximum length ~ 3.9 mm.

netti 2012). Within the genus *Phlaeopterus* Motschulsky, 1853, are five species with maximum body lengths over 8 mm, and one species, *P. bakerensis*, with a maximum body size of ~10 mm. There is considerable body size variation within the genus, with the largest species being over twice the length of the smallest species (Figs 1, 2). The genus contains 22 species (Mullen et al. 2018; Shavrin 2020), and is distributed across mountainous regions of northwestern North America and eastern Asia (Fig. 3). *Phlaeopterus* occur primarily along the edges of alpine snowfields and cold, cascading streams and waterfalls up to 3,830 meters in elevation (Mullen et al. 2018). *Phlaeopterus* adults have been observed foraging on arthropod fallout on the surface of alpine snowfields, mostly flying insects, windblown from lower elevations and often lethargic or frozen (Mullen et al. 2018).

The genus was erected with minimal diagnosis by Motschulsky (1853) based on the species *Phlaeopterus fusconiger* Motschulsky, 1853. Additional species were described or transferred by Fauvel (1878), Casey (1885, 1886, 1893), Hatch (1957), Rougemont (2000), Shavrin (2001), Shavrin and Mullen (2015), and Mullen et al. (2018). Shavrin and Mullen's (2015) transfer of one Siberian *Lesteva* Latreille, 1797 species into *Phlaeopterus* made the originally Nearctic genus Holarctic. Mullen et al. (2018) revised the genus, described eight new species, and synonymized the monotypic genus *Vellica* Casey, 1885 under *Phlaeopterus*, bringing the species count to 18. Shavrin (2020) transferred three species from *Lesteva* into *Phlaeopterus* and described a new species, all from China, bringing the total for the genus to 22 species. Diagnoses of the genus have been published by Hatch (1957), Moore and Legner (1979), Newton et al. (2000), Shavrin and Mullen (2015) and Mullen et al. (2018). More details on the taxonomic history of the group are provided in Mullen et al. (2018). A summary of taxonomic hypotheses of previous authors and previously unpublished species-group hypotheses is provided in Table 1; notable among these is a hypothesis that the 13 large-bodied species (maximum size over 5 mm) descended from a single large-bodied common ancestor. The unpublished species group hypotheses in Table 1 were originally proposed by J.M. Campbell based on morphological characters that were used in part, modified, and added to in our morphological dataset.

Here, we present the first phylogenetic analyses of species relationships within *Phlaeopterus*. Our primary goals were to: 1) estimate the phylogeny of the genus, 2) assess if morphology-based species demarcations correspond to discrete mtDNA lineages, 3) test prior hypotheses of

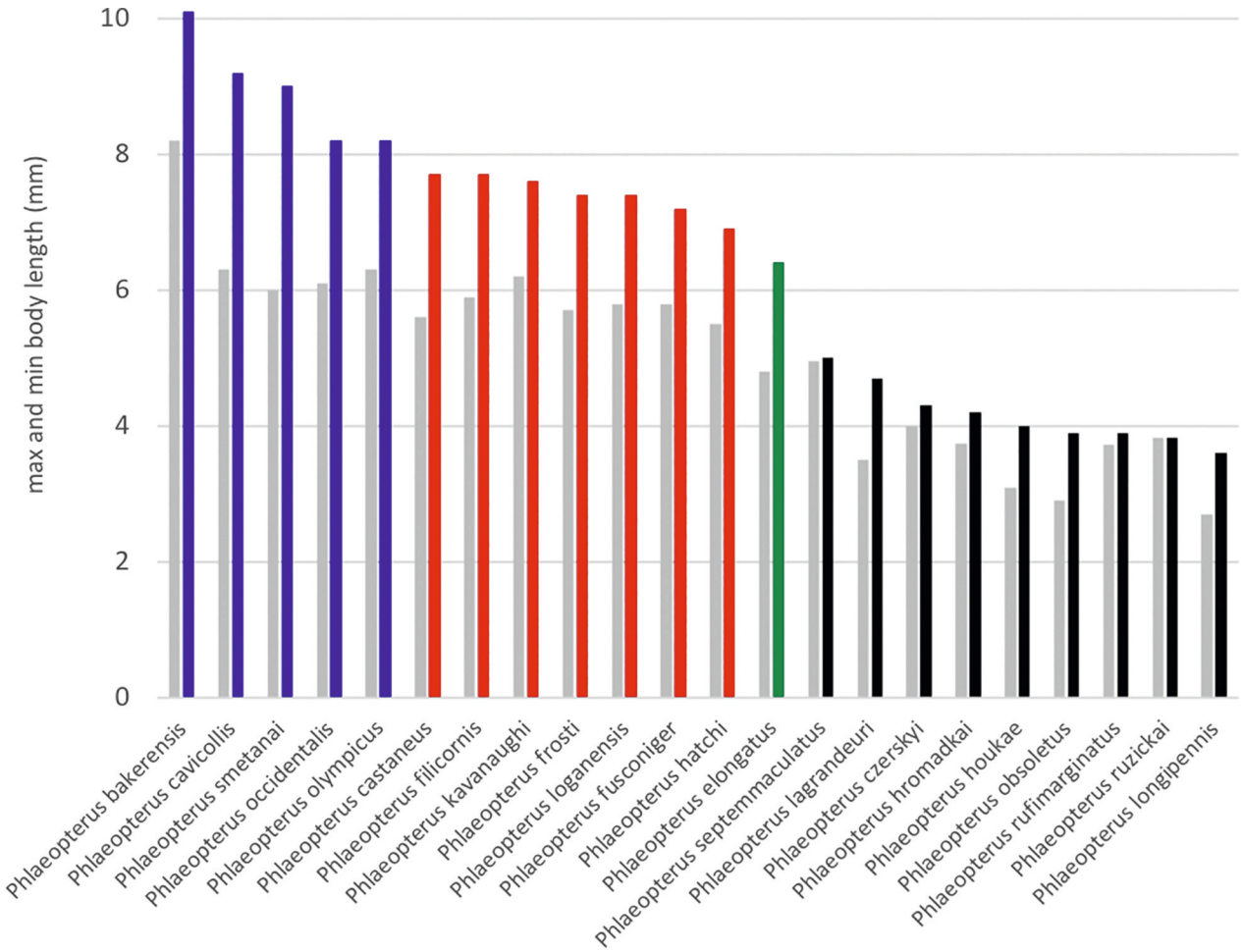

Figure 2. Minimum (grey columns) and maximum (blue, red, green, and black columns) body lengths of *Phlaeopterus* species sorted from largest to smallest maximum length. Bars in blue are species with maximum body sizes over 8 mm; bars in red are species with maximum body sizes 6.5 to 7.9 mm with wide bodies; bars in black are species with maximum body sizes below 5 mm; the green bar is for *P. elongatus* with a maximum body size of 6.4 mm, with an elongate body. Data from Mullen et al. (2018) and Shavrin (2020).

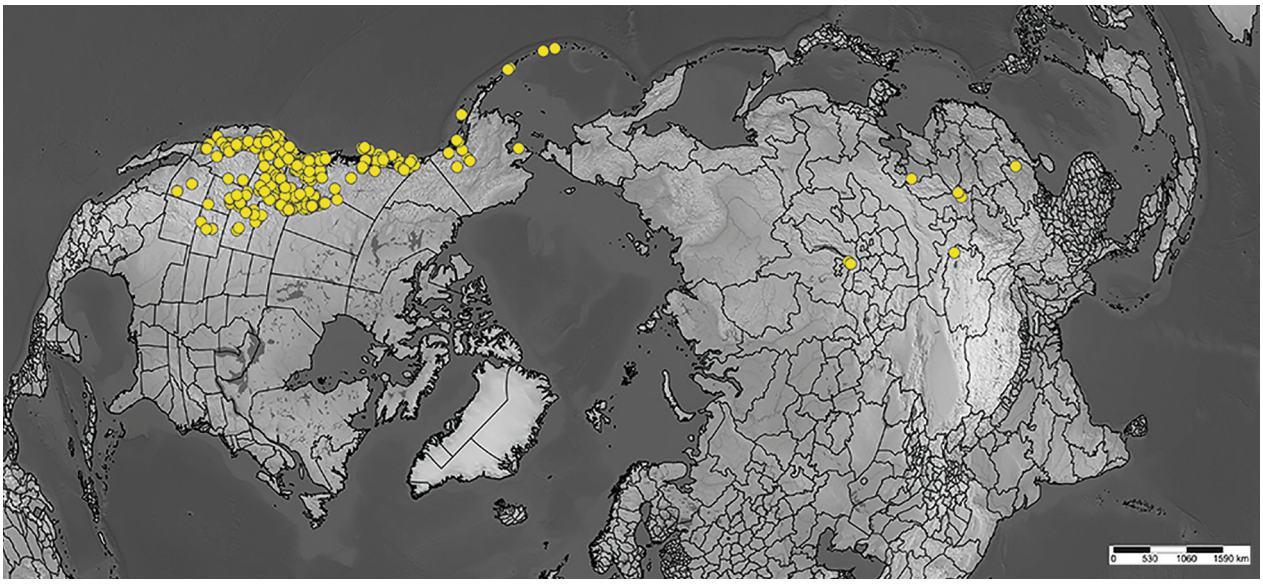

Figure 3. Distribution of the genus *Phlaeopterus* based on over 2,000 georeferenced records visualized with SimpleMappr (Short-house 2010).

species relationships within *Phlaeopterus*, and 4) understand the evolution of large body size in the genus. We were explicitly not attempting to test the monophyly of the genus *Phlaeopterus*, nor infer its relationship to other genera in the tribe Anthophagini Thompson 1859, which would require much greater taxon and character sam-

Table 1. Taxonomic hypotheses of the genus *Phlaeopterus*. g = genus, sg = informal species group. Most of these species groups were proposed by J.M. Campbell in his unpublished cladistic study on *Phlaeopterus*.

Hypothesis	Author (concept)	Taxa included
Tilea g	Fauvel (1878)	*P. cavicollis* (outside *Phlaeopterus*)
Vellica g	Casey (1885)	*P. longipennis* (outside *Phlaeopterus*)
longipennis sg	Campbell unpublished	*P. longipennis, P. obsoletus*
castaneus sg	Campbell unpublished	*P. castaneus, P. kavanaughi*
cavicollis sg	Campbell unpublished	*P. cavicollis, P. bakerensis, P. smetanai*
fusconiger sg	Campbell unpublished	*P. occidentalis, P. olympicus, P. loganensis, P. fusconiger, P. frosti*
filicornis sg	Campbell unpublished	*P. filicornis, P. hatchi, P. elongatus*
Phlaeopterus sensu stricto	Campbell unpublished	all species with maximum body size over 5 mm

pling. However, our taxon sampling did allow a weak test of the monophyly of the genus *Phlaeopterus*.

2. Materials and methods

2.1. Taxon sampling

Our morphological data set contains 18 of the 22 *Phlaeopterus* species, and nine of these are represented in our molecular dataset (Table 2). The three Chinese species recently transferred from *Lesteva* to *Phlaeopterus* and the new species described by Shavrin (2020), *Phlaeopterus rufimarginatus* (Rougemont, 2000), *Phlaeopterus ruzickai* (Shavrin, 2015), *Phlaeopterus septemmaculatus* (Rougemont, 2000), and *Phlaeopterus hromadkai* Shavrin, 2020, were not included in our analyses, which were based on data obtained before publication of Shavrin (2020). However, our dataset includes one Palearctic species, *Phlaeopterus czerskyi* (Shavrin, 2001).

Wherever possible, multiple exemplars of each *Phlaeopterus* species were included in our molecular dataset, with specimens selected from the widest available geographic range for each species. Geographic ranges were estimated based on study of borrowed museum specimens. Of over 2,000 museum specimens databased (http://arctos.database.museum/saved/Phlaeopterus) each species was represented by an average of 142.2 specimens for these range estimates (range: 2–325 specimens/species). We prepared the map in Fig. 3 using these data with SimpleMappr (Shorthouse 2010). Repository details for these specimens can be found in Mullen et al. (2018). Our outgroup for the morphological dataset is composed of four *Lesteva* and one *Unamis* Casey, 1894 species, the latter corresponding to the same *Unamis* species for which we could obtain a DNA barcode sequence. Our outgroup for the molecular dataset is composed of all the publicly available *Lesteva* (six species) and *Unamis* (one sequence identified to species and two identified to genus) DNA barcode sequences that were available at the time, and those we generated, on BOLD. *Lesteva* and *Unamis* were selected as outgroup taxa based on their morphological similarity to *Phlaeopterus* (Moore and Legner 1979) and because all three genera belong to the tribe Anthophagini (Newton et al. 2000).

2.2. Morphological data

Our morphological dataset contains 35 external and 5 male genitalic characters, the majority of which derive from the unpublished work of J.M. Campbell. Character 35 was modified from Moore and Legner (1979). Some of Campbell's original characters were modified after our study and measurements of specimens led us to disagree with his codings (e.g. character 9, interfacetal setae of eye, was changed from a three-state character to a two-state character). Codings reflect hypotheses of homology among species, although some characters are notable autapomorphies. When doubt existed about the homology of states in certain taxa those taxa were coded as 'missing/inapplicable' for those characters. Continuous characters such as ratios of lengths were evaluated to find gaps among species which were used to assign states. Within-species polymorphism was handled by assigning the majority state to that species when the state was clearly in the majority or assigning a separate state for the presence of polymorphism (e.g. character 30). When no state was in the clear majority, the species was coded as polymorphic with both states (for instance, *P. lagrandeuri* Hatch, 1957 in character 27). Polymorphism of length characters within a species was handled by using the average of multiple measurements. All characters of potential phylogenetic value were included even if some were missing data.

We observed characters with a Leica M165 C stereomicroscope (Leica Microsystems, Wetzlar, Germany), and coded morphological data in Mesquite 3.6 (Maddison and Maddison 2016). Our morphological data matrix and trees are archived at http://purl.org/phylo/treebase/phylows/study/TB2:S27393 and among Supplementary files S1, S2, and S3. Length data for character 16 were analyzed statistically using R version 4.0.0 (R Core Team 2020) in RStudio version 1.2.5042 (RStudio Team 2020) during the character coding process.

We coded characters from type specimens whenever possible, and specimens determined primarily by J.M. Campbell belonging to, or on loan to, the University of Alaska Museum Insect Collection from the California Academy of Sciences, San Francisco, California (David H. Kavanaugh, Jere Schweikert) and the Canadian National Collection of Insects, Ottawa, Ontario, Canada (Patrice Bouchard, Anthony Davies).

Table 2. COI sequences used in this study.

Taxon	Process ID	BIN	Catalog Num	Seq. Length	Country	State/Province	Locality
Lesteva longoelytrata	FBCOA209-10	BOLD:AAX5588	BFB_Col_FK_0209	658[0n]	Germany	North Rhine-Westphalia	Bornheim-Brenig, Sandgrube
Lesteva longoelytrata	FBCOE1134-12	BOLD:AAX5588	BFB_Col_FK_3604	658[0n]	Germany	Bavaria	Collenberg-Kirschfurt, Kiesgruben
Lesteva longoelytrata	FBCOP868-13	BOLD:AAX5588	BFB_Col_FK_9822	658[0n]	Germany	North Rhine-Westphalia	Schleiden-Wolfgarten, Kermeter Mariawald
Lesteva longoelytrata	GBCOC286-12	BOLD:AAX5588	GBOL_Col_FK_1521	647[0n]	Germany	Rhineland-Palatinate	Altenahr-Berg, Oberes Vischeltal
Lesteva longoelytrata	GBCOL247-12	BOLD:AAX5588	GBOL_Col_FK_2812	658[0n]	Germany	Saxony	Chemnitz-Hilbersdorf, Orchideenwiese
Lesteva longoelytrata	GBCOL896-12	BOLD:AAX5588	GBOL_Col_FK_3746	658[0n]	Germany	Rhineland-Palatinate	Kastellaun, Wohnrother Bach
Lesteva longoelytrata	GCOL10283-16	BOLD:AAX5588	ZFMK-TIS-2524050	658[0n]	Germany	Saxony-Anhalt	Athenstedt
Lesteva longoelytrata	GCOL10320-16	BOLD:AAX5588	ZFMK-TIS-2524127	658[0n]	Germany	Saxony-Anhalt	Athenstedt
Lesteva longoelytrata	GCOL11168-16	BOLD:AAX5588	ZFMK-TIS-2529113	658[0n]	Germany	Saxony	Zeisigwald
Lesteva longoelytrata	GCOL12150-16	BOLD:AAX5588	ZFMK-TIS-2532908	658[0n]	Germany	Bavaria	Haeuseloher Moor
Lesteva longoelytrata	GCOL12151-16	BOLD:AAX5588	ZFMK-TIS-2532909	658[0n]	Germany	Bavaria	Haeuseloher Moor
Lesteva longoelytrata	GCOL12170-16	BOLD:AAX5588	ZFMK-TIS-2532951	658[0n]	Germany	Saxony	NSG Maylust
Lesteva longoelytrata	GCOL13450-16	BOLD:AAX5588	ZFMK-TIS-2556258	658[0n]	Germany	Mecklenburg-Vorpommern	Autokescher S1: Babke-Zartwitz-Speck-Schwarzenhof
Lesteva longoelytrata	GCOL13466-16	BOLD:AAX5588	ZFMK-TIS-2556281	658[0n]	Germany	Mecklenburg-Vorpommern	Autokescher S1: Babke-Zartwitz-Speck-Schwarzenhof
Lesteva longoelytrata	GCOL13476-16	BOLD:AAX5588	ZFMK-TIS-2556301	658[0n]	Germany	Mecklenburg-Vorpommern	Autokescher S1: Babke-Zartwitz-Speck-Schwarzenhof
Lesteva longoelytrata	GCOL3231-16	BOLD:AAX5588	ZFMK-TIS-16853	658[0n]	Germany	Saxony	NSG Eichberg
Lesteva longoelytrata	GCOL5495-16	BOLD:AAX5588	ZFMK-TIS-2503942	658[0n]	Germany	Thuringia	Dietlas/Merkers, S, Felda-Ufer
Lesteva longoelytrata	GCOL5505-16	BOLD:AAX5588	ZFMK-TIS-2503954	658[0n]	Germany	Thuringia	Dietlas/Merkers, S, Felda-Ufer
Lesteva longoelytrata	GCOL5507-16	BOLD:AAX5588	ZFMK-TIS-2503956	658[0n]	Germany	Thuringia	Dietlas/Merkers, S, Felda-Ufer
Lesteva longoelytrata	GCOL5524-16	BOLD:AAX5588	ZFMK-TIS-2503980	658[0n]	Germany	Thuringia	Dietlas/Merkers, S, Felda-Ufer
Lesteva monticola	COLFE916-13	BOLD:ACG0938	ZMUO.006236	658[0n]	Finland		Rautuvaara
Lesteva monticola	COLFE917-13	BOLD:ACG0938	ZMUO.006237	658[0n]	Finland		Rautuvaara
Lesteva monticola	FBCOD706-11	BOLD:ABA6559	BFB_Col_FK_2511	658[0n]	Italy	Trentino-Alto Adige	Moos, Kreuzbergpass
Lesteva monticola	FBCOD707-11	BOLD:ABA6559	BFB_Col_FK_2512	658[0n]	Italy	Trentino-Alto Adige	Moos, Kreuzbergpass
Lesteva pallipes	ASALC492-13	BOLD:ACI6270		658[0n]	Canada	Ontario	Cut
Lesteva pallipes	ELPCG287-17	BOLD:ACI6270	L#17PHCOT-0006	588[0n]	Canada	Ontario	Eel Lake Cottage
Lesteva pallipes	SSKJC2422-15	BOLD:ACI6270	BIOUG19505-A09	588[0n]	Canada	Nova Scotia	
Lesteva pubescens	FBCOD729-11	BOLD:ABA6561	BFB_Col_FK_2534	658[0n]	Italy	Trentino-Alto Adige	Innichen, Sextenbach
Lesteva pubescens	FBCOD730-11	BOLD:ABA6561	BFB_Col_FK_2535	658[0n]	Italy	Trentino-Alto Adige	Innichen, Sextenbach
Lesteva pubescens	GCOL8143-16	BOLD:ABA6561	ZFMK-TIS-2512508	658[0n]	Germany	North Rhine-Westphalia	Urftaue
Lesteva pubescens	GCOL8144-16	BOLD:ABA6561	ZFMK-TIS-2512509	658[0n]	Germany	North Rhine-Westphalia	Urftaue
Lesteva punctata	FBCOF541-12	BOLD:ABY1451	BFB_Col_FK_4151	596[0n]	Germany	Rhineland-Palatinate	Neuburg, Altrheine
Lesteva punctata	FBCOF542-12	BOLD:ABY1451	BFB_Col_FK_4152	658[0n]	Germany	Rhineland-Palatinate	Neuburg, Altrheine
Lesteva punctata	FBCOI588-12	BOLD:ABY1451	BFB_Col_FK_8568	658[0n]	Germany	Rhineland-Palatinate	Neuburg, Lautermuendung
Lesteva punctata	FBCOP178-13	BOLD:ABY1451	BFB_Col_FK_10177	658[5n]	Germany	Rhineland-Palatinate	Kastellaun, Wohnrother Bach

Table 2 continued.

Taxon	Process ID	BIN	Catalog Num	Seq. Length	Country	State/Province	Locality
Lesteva punctata	GCOL5603-16	BOLD:ABY1451	ZFMK-TIS-2504075	658[0n]	Germany	Thuringia	Wilhelmsthal/Eisenach, Fischteiche
Lesteva punctata	GCOL5604-16	BOLD:ABY1451	ZFMK-TIS-2504076	658[0n]	Germany	Thuringia	Wilhelmsthal/Eisenach, Fischteiche
Lesteva punctata	GCOL8448-16	BOLD:ABY1451	ZFMK-TIS-2515316	658[0n]	Germany	North Rhine-Westphalia	Wuestebach
Lesteva punctata	GCOL8450-16	BOLD:ABY1451	ZFMK-TIS-2515320	658[1n]	Germany	North Rhine-Westphalia	Wuestebach
Lesteva sicula	FBCOA005-10	BOLD:ABW6647	BFB_Col_FK_0100	658[0n]	Germany	North Rhine-Westphalia	Wesel-Diersfordt, Schnepfenberge
Lesteva sicula	FBCOE387-12	BOLD:ABW6647	BFB_Col_FK_4377	658[0n]	Germany	North Rhine-Westphalia	Roetgen, Inde
Lesteva sicula	FBCOH854-12	BOLD:ABW6647	BFB_Col_FK_6743	658[0n]	Germany	North Rhine-Westphalia	Arnsberg-Breitenbruch, NWZ Hellerberg
Lesteva sicula	FBCOP590-13	BOLD:ABW6647	BFB_Col_FK_11159	658[0n]	Germany	Saxony-Anhalt	Seeburg-Rollsdorf, Bindersee
Lesteva sicula	FBCOP591-13	BOLD:ABW6647	BFB_Col_FK_11160	658[0n]	Germany	Saxony-Anhalt	Seeburg-Rollsdorf, Bindersee
Lesteva sicula	GBCOF813-13	BOLD:ABW6647	GBOL_Col_FK_4898	658[0n]	Germany	Saxony-Anhalt	Seeburg-Rollsdorf, Bindersee
Lesteva sicula	GBCOF814-13	BOLD:ABW6647	GBOL_Col_FK_4899	658[0n]	Germany	Saxony-Anhalt	Seeburg-Rollsdorf, Bindersee
Lesteva sicula	GCOL13439-16	BOLD:ABW6647	ZFMK-TIS-2556243	658[0n]	Germany	Mecklenburg-Vorpommern	Autokescher S1: Babke-Zartwitz-Speck-Schwarzenhof
Lesteva sicula	GCOL8492-16	BOLD:ABW6647	ZFMK-TIS-2515434	658[0n]	Germany	North Rhine-Westphalia	Fuhrtsbachtal
Phlaeopterus	BBCCN675-10	BOLD:AAP7088	10PCCOL-0580	658[0n]	Canada	British Columbia	
Phlaeopterus	SSGLB3519-15	BOLD:AAP7088	BIOUG26715-B08	537[0n]	Canada	British Columbia	Hemlock Grove Boardwalk
Phlaeopterus	SSGLB3520-15	BOLD:AAP7088	BIOUG26715-B09	579[0n]	Canada	British Columbia	Hemlock Grove Boardwalk
Phlaeopterus	SSGLB3526-15	BOLD:AAP7088	BIOUG26715-C03	567[0n]	Canada	British Columbia	Hemlock Grove Boardwalk
Phlaeopterus	SSGLC1659-15	BOLD:AAP7088	BIOUG22200-F12	549[0n]	Canada	British Columbia	Meeting of the Waters Trail
Phlaeopterus	SSGLC1783-15	BOLD:AAP7088	BIOUG22311-H04	588[0n]	Canada	British Columbia	Meeting of the Waters Trail
Phlaeopterus	SSGLC1786-15	BOLD:AAP7088	BIOUG22311-H07	588[0n]	Canada	British Columbia	Meeting of the Waters Trail
Phlaeopterus	SSGLC1816-15	BOLD:AAP7088	BIOUG22339-C02	576[0n]	Canada	British Columbia	Meeting of the Waters Trail
Phlaeopterus	SSGLC1853-15	BOLD:AAP7088	BIOUG22339-F03	579[0n]	Canada	British Columbia	Meeting of the Waters Trail
Phlaeopterus	SSGLC1865-15	BOLD:AAP7088	BIOUG22339-G03	591[0n]	Canada	British Columbia	Meeting of the Waters Trail
Phlaeopterus	SSGLC2028-15	BOLD:AAP7088	BIOUG22341-D12	576[0n]	Canada	British Columbia	Meeting of the Waters Trail
Phlaeopterus	SSGLC2069-15	BOLD:AAP7088	BIOUG22341-H05	576[0n]	Canada	British Columbia	Meeting of the Waters Trail
Phlaeopterus	SSGLC2077-15	BOLD:AAP7088	BIOUG22342-A02	570[0n]	Canada	British Columbia	Meeting of the Waters Trail
Phlaeopterus	SSGLC2078-15	BOLD:AAP7088	BIOUG22342-A03	588[0n]	Canada	British Columbia	Meeting of the Waters Trail
Phlaeopterus	SSGLC2084-15	BOLD:AAP7088	BIOUG22342-A09	579[0n]	Canada	British Columbia	Meeting of the Waters Trail
Phlaeopterus	SSGLC2091-15	BOLD:AAP7088	BIOUG22342-B04	576[0n]	Canada	British Columbia	Meeting of the Waters Trail
Phlaeopterus	SSGLC2407-15	BOLD:AAP7088	BIOUG22371-A05	582[0n]	Canada	British Columbia	Meeting of the Waters Trail
Phlaeopterus castaneus	PHLA071-20	BOLD:AAP7088	UAM:Ento:317804	658[0n]	United States	Idaho	Seven Devils Campground and Seven Devils Lake
Phlaeopterus castaneus	SSGLC1658-15	BOLD:AAP7088	BIOUG22200-F11	579[0n]	Canada	British Columbia	Meeting of the Waters Trail
Phlaeopterus castaneus	SSGLC1660-15	BOLD:AAP7088	BIOUG22200-G01	567[0n]	Canada	British Columbia	Meeting of the Waters Trail
Phlaeopterus castaneus	SSGLC1661-15	BOLD:AAP7088	BIOUG22200-G02	567[0n]	Canada	British Columbia	Meeting of the Waters Trail
Phlaeopterus castaneus cascadiensis	UAMIC1108-13	BOLD:ACH1347	UAM:Ento:132746	658[0n]	United States	Alaska	Haines, Flower Mtn

Table 2 continued.

Taxon	Process ID	BIN	Catalog Num	Seq. Length	Country	State/Province	Locality
Phlaeopterus castaneus cascadiensis	PHLA032-20	BOLD:ACH1347	UAM:Ento:303785	654[0n]	Canada	British Columbia	Brohm Ridge
Phlaeopterus cavicollis	PHLA018-20	BOLD:ACS6522	UAM:Ento:254996	638[0n]	United States	Alaska	S. Baranof Is. E. of Snipe Bay
Phlaeopterus cavicollis	PHLA019-20	BOLD:ACS6522	UAM:Ento:256230	638[0n]	United States	Alaska	Mahoney Mt.
Phlaeopterus cavicollis	PHLA020-20	BOLD:ACS6522	UAM:Ento:256231	638[0n]	United States	Alaska	Mahoney Mt.
Phlaeopterus cavicollis	PHLA021-20	BOLD:ACS6522	UAM:Ento:256233	636[0n]	United States	Alaska	Mahoney Mt.
Phlaeopterus cavicollis	PHLA022-20	BOLD:ACS6522	UAM:Ento:256234	634[0n]	United States	Alaska	Mahoney Mt.
Phlaeopterus cavicollis	PHLA023-20	BOLD:ACS6522	UAM:Ento:256238	652[0n]	United States	Alaska	Mahoney Mt.
Phlaeopterus cavicollis	PHLA024-20	BOLD:ACS6522	UAM:Ento:256241	638[0n]	United States	Alaska	Mahoney Mt.
Phlaeopterus cavicollis	PHLA025-20	BOLD:ACS6522	UAM:Ento:256251	639[0n]	United States	Alaska	Mahoney Mt.
Phlaeopterus cavicollis	PHLA026-20	BOLD:ACS6522	UAMObs:Ento:231988	658[0n]	United States	California	Riverside Co. SanBernardinoNF: Fuller`s Ridge Trlhd.
Phlaeopterus cavicollis	PHLA027-20	BOLD:ACS6522	UAMObs:Ento:231996	633[0n]	United States	California	Kern Co. Los PadresNF, Mt. Pinos
Phlaeopterus cavicollis	PHLA028-20	BOLD:ACS6522	UAMObs:Ento:232004	658[0n]	United States	California	Nevada Co.: Carpenter Ridge
Phlaeopterus cavicollis	PHLA056-20	BOLD:ACS6522	UAMObs:Ento:232734	658[0n]	United States	Washington	Olympic National Park, north slope of Mount Olympus at Snow Dome
Phlaeopterus cavicollis	PHLA057-20	BOLD:ACS6522	UAMObs:Ento:232735	658[0n]	United States	California	Tulare Co., Kings Cyn. NP
Phlaeopterus cavicollis	PHLA058-20	BOLD:ACS6522	UAMObs:Ento:232736	655[0n]	United States	California	El Dorado County, Lilly Lake
Phlaeopterus cavicollis	PHLA059-20	BOLD:ACS6522	UAMObs:Ento:232737	658[0n]	United States	California	El Dorado County, Lilly Lake
Phlaeopterus cavicollis	PHLA060-20	BOLD:ACS6522	UAMObs:Ento:232738	658[0n]	United States	California	El Dorado County, Lilly Lake
Phlaeopterus cavicollis	PHLA061-20	BOLD:ACS6522	UAMObs:Ento:232739	658[0n]	United States	California	El Dorado County, Lilly Lake
Phlaeopterus cavicollis	PHLA063-20	BOLD:ACS6522	UAMObs:Ento:232741	652[0n]	United States	Washington	Olympic National Park, north slope of Mount Olympus at Snow Dome
Phlaeopterus cavicollis	UAMIC2290-14	BOLD:ACS6522	UAM:Ento:254995	658[0n]	United States	Alaska	S. Baranof Is. E. of Snipe Bay
Phlaeopterus cavicollis	UAMIC2294-14	BOLD:ACS6522	UAM:Ento:275766	658[0n]	United States	Alaska	Hawthorne Peak
Phlaeopterus cavicollis	UAMIC2305-14	BOLD:ACS6522	UAM:Ento:256236	658[0n]	United States	Alaska	Mahoney Mt.
Phlaeopterus cavicollis	UAMIC2374-14	BOLD:ACS6522	UAM:Ento:275765	658[0n]	United States	Alaska	Hawthorne Peak
Phlaeopterus elongatus	PHLA033-20	BOLD:AEE6845	UAM:Ento:303798	651[0n]	United States	Alaska	Alaska Range, Antimony Creek
Phlaeopterus elongatus	PHLA034-20	BOLD:AEE6845	UAM:Ento:303799	630[0n]	United States	Alaska	Alaska Range, Antimony Creek
Phlaeopterus elongatus	PHLA035-20	BOLD:AEE6845	UAM:Ento:303801	658[0n]	United States	Alaska	Alaska Range, Antimony Creek
Phlaeopterus elongatus	PHLA036-20	BOLD:AEE6845	UAM:Ento:303802	658[0n]	United States	Alaska	Alaska Range, Antimony Creek
Phlaeopterus elongatus	PHLA037-20	BOLD:AEE6845	UAM:Ento:303803	633[0n]	United States	Alaska	Summit Lake
Phlaeopterus elongatus	PHLA038-20	BOLD:AEE6845	UAM:Ento:303804	655[0n]	United States	Alaska	Summit Lake
Phlaeopterus elongatus	PHLA039-20	BOLD:AEE6845	UAM:Ento:303805	631[0n]	United States	Alaska	Summit Lake
Phlaeopterus elongatus	PHLA040-20	BOLD:AEE6845	UAM:Ento:303806	655[0n]	United States	Alaska	Summit Lake
Phlaeopterus elongatus	PHLA041-20	BOLD:AEE6845	UAM:Ento:303810	632[0n]	United States	Alaska	Summit Lake
Phlaeopterus elongatus	PHLA042-20	BOLD:AEE6845	UAM:Ento:303811	658[0n]	United States	Alaska	Summit Lake
Phlaeopterus fusconiger	PHLA001-20	BOLD:ACH1373	UAM:Ento:151002	637[0n]	United States	Alaska	Juneau, Heintzleman Ridge

Table 2 continued.

Taxon	Process ID	BIN	Catalog Num	Seq. Length	Country	State/Province	Locality
Phlaeopterus fusconiger	PHLA002-20	BOLD:ACH1373	UAM:Ento:151004	637[0n]	United States	Alaska	Juneau, Heintzleman Ridge
Phlaeopterus fusconiger	PHLA003-20	BOLD:ACH1373	UAM:Ento:149865	640[0n]	United States	Alaska	Heintzleman Ridge, pl.01
Phlaeopterus fusconiger	PHLA004-20	BOLD:ACH1373	UAM:Ento:147759	638[0n]	United States	Alaska	S. Chilkat Range
Phlaeopterus fusconiger	PHLA005-20	BOLD:ACH1373	UAM:Ento:147764	638[0n]	United States	Alaska	S. Chilkat Range
Phlaeopterus fusconiger	PHLA006-20	BOLD:ACH1373	UAM:Ento:147808	632[0n]	United States	Alaska	S. Chilkat Range
Phlaeopterus fusconiger	PHLA007-20	BOLD:ACH1373	UAM:Ento:147810	637[0n]	United States	Alaska	S. Chilkat Range
Phlaeopterus fusconiger	PHLA008-20	BOLD:ACH1373	UAM:Ento:149862	637[0n]	United States	Alaska	Heintzleman Ridge, pl.01
Phlaeopterus fusconiger	PHLA009-20	BOLD:ACH1373	UAM:Ento:149863	638[0n]	United States	Alaska	Heintzleman Ridge, pl.01
Phlaeopterus fusconiger	PHLA010-20	BOLD:ACH1373	UAM:Ento:149864	638[0n]	United States	Alaska	Heintzleman Ridge, pl.01
Phlaeopterus fusconiger	PHLA011-20	BOLD:ACH1373	UAM:Ento:149916	638[0n]	United States	Alaska	Heintzleman Ridge, pl.07
Phlaeopterus fusconiger	PHLA012-20	BOLD:ACH1373	UAM:Ento:150994	639[0n]	United States	Alaska	Juneau, Heintzleman Ridge
Phlaeopterus fusconiger	PHLA013-20	BOLD:ACH1373	UAM:Ento:151000	631[0n]	United States	Alaska	Juneau, Heintzleman Ridge
Phlaeopterus fusconiger	PHLA014-20	BOLD:ACH1373	UAM:Ento:151003	638[0n]	United States	Alaska	Juneau, Heintzleman Ridge
Phlaeopterus fusconiger	PHLA015-20	BOLD:ACH1373	UAM:Ento:151006	630[0n]	United States	Alaska	Juneau, Heintzleman Ridge
Phlaeopterus fusconiger	PHLA016-20	BOLD:ACH1373	UAM:Ento:151007	635[0n]	United States	Alaska	Juneau, Heintzleman Ridge
Phlaeopterus fusconiger	PHLA029-20	BOLD:ACH1373	UAM:Ento:258286	632[0n]	United States	Alaska	Chichagof Is.
Phlaeopterus fusconiger	PHLA043-20	BOLD:ACH1373	UAM:Ento:303814	658[0n]	United States	Alaska	Takshanuk Mountains, NW of Haines
Phlaeopterus fusconiger	PHLA044-20	BOLD:ACH1373	UAM:Ento:303815	643[0n]	United States	Alaska	Takshanuk Mountains, NW of Haines
Phlaeopterus fusconiger	PHLA045-20	BOLD:ACH1373	UAM:Ento:303817	632[0n]	United States	Alaska	Takshanuk Mountains, NW of Haines
Phlaeopterus fusconiger	PHLA046-20	BOLD:ACH1373	UAM:Ento:303818	658[0n]	United States	Alaska	Takshanuk Mountains, NW of Haines
Phlaeopterus fusconiger	PHLA047-20	BOLD:ACH1373	UAM:Ento:303819	637[0n]	United States	Alaska	Takshanuk Mountains, NW of Haines
Phlaeopterus fusconiger	PHLA048-20	BOLD:ACH1373	UAM:Ento:303822	633[0n]	United States	Alaska	Takshanuk Mountains
Phlaeopterus fusconiger	PHLA049-20	BOLD:ACH1373	UAM:Ento:303823	633[0n]	United States	Alaska	Takshanuk Mountains
Phlaeopterus fusconiger	PHLA050-20	BOLD:ACH1373	UAM:Ento:303824	648[0n]	United States	Alaska	Takshanuk Mountains
Phlaeopterus fusconiger	PHLA051-20	BOLD:ACH1373	UAM:Ento:303825	632[0n]	United States	Alaska	Takshanuk Mountains
Phlaeopterus fusconiger	PHLA052-20	BOLD:ACH1373	UAM:Ento:303827	643[0n]	United States	Alaska	Takshanuk Mountains
Phlaeopterus fusconiger	PHLA053-20	BOLD:ACH1373	UAM:Ento:303828	645[0n]	United States	Alaska	Takshanuk Mountains
Phlaeopterus fusconiger	PHLA054-20	BOLD:ACH1373	UAM:Ento:303829	634[0n]	United States	Alaska	north end of Paradise Valley (between Bucher and Gilkey Glaciers)
Phlaeopterus fusconiger	PHLA062-20	BOLD:ACH1373	UAMObs:Ento:232740	654[0n]	United States	Washington	Olympic National Park, north slope of Mount Olympus at Snow Dome
Phlaeopterus fusconiger	PHLA067-20	BOLD:ACH1373	UAM:Ento:317327	657[0n]	United States	Alaska	Adak Island, Mt. Moffett
Phlaeopterus fusconiger	PHLA068-20	BOLD:ACH1373	UAM:Ento:317328	658[0n]	United States	Alaska	Adak Island, Mt. Moffett
Phlaeopterus fusconiger	PHLA069-20		UAM:Ento:317329	658[0n]	United States	Alaska	Adak Island, Mt. Moffett
Phlaeopterus fusconiger	UAMIC1120-13	BOLD:ACH1373	UAM:Ento:151001	658[0n]	United States	Alaska	Juneau, Heintzleman Ridge
Phlaeopterus fusconiger	UAMIC1121-13	BOLD:ACH1373	UAM:Ento:151005	658[0n]	United States	Alaska	Juneau, Heintzleman Ridge

Table 2 continued.

Taxon	Process ID	BIN	Catalog Num	Seq. Length	Country	State/Province	Locality
Phlaeopterus houkae	BMAPH046-15	BOLD:ACP3648	SC14-116-03	633[2n]	Canada	British Columbia	
Phlaeopterus houkae	PHLA017-20	BOLD:ACP3648	UAM:Ento:152322	658[0n]	United States	Alaska	Juneau, Heintzleman Ridge
Phlaeopterus houkae	PHLA030-20	BOLD:ACP3648	UAM:Ento:275535	658[0n]	United States	Alaska	Hawthorne Peak pl.20
Phlaeopterus houkae	UAMIC2293-14	BOLD:ACP3648	UAM:Ento:275545	558[0n]	United States	Alaska	Hawthorne Peak
Phlaeopterus houkae	UAMIC2310-14	BOLD:ACP3648	UAM:Ento:153501	651[0n]	United States	Alaska	S. Chilkat Pen. pl.18
Phlaeopterus houkae	UAMIC2369-14	BOLD:ACP3648	UAM:Ento:152317	658[0n]	United States	Alaska	Juneau, Heintzleman Ridge
Phlaeopterus houkae	UAMIC2373-14	BOLD:ACP3648	UAM:Ento:275534	658[0n]	United States	Alaska	Hawthorne Peak pl.20
Phlaeopterus kavanaughi	PHLA055-20	BOLD:AEE3708	UAMObs:Ento:232733	658[0n]	United States	California	Trinity County, Trinity Alps, Canyon Creek snowfield
Phlaeopterus kavanaughi	PHLA064-20	BOLD:AEE3708	UAMObs:Ento:232745	652[0n]	United States	California	Siskiyou County, Trinity Alps, Salmon Glacier
Phlaeopterus lagrandeuri	CNRVG2709-15	BOLD:ACE7299	BIOUG20368-D03	564[1n]	Canada	British Columbia	
Phlaeopterus lagrandeuri	CNRVG2714-15	BOLD:ACE7299	BIOUG20368-D08	606[0n]	Canada	British Columbia	
Phlaeopterus lagrandeuri	CNRVG2717-15	BOLD:ACE7299	BIOUG20368-D11	546[0n]	Canada	British Columbia	
Phlaeopterus lagrandeuri	GMNCJ156-13	BOLD:ACE7299	BIOUG06773-C11	670[0n]	United States	Washington	Enivornmental Learning Centre
Phlaeopterus lagrandeuri	PHLA031-20	BOLD:ACE7299	UAM:Ento:303784	634[0n]	Canada	British Columbia	Brohm Ridge
Phlaeopterus lagrandeuri	SSGLC2022-15	BOLD:ACE7299	BIOUG22341-D06	576[0n]	Canada	British Columbia	Meeting of the Waters Trail
Phlaeopterus lagrandeuri	SSGLC2138-15	BOLD:ACE7299	BIOUG22342-F03	576[0n]	Canada	British Columbia	Meeting of the Waters Trail
Phlaeopterus lagrandeuri	SSGLC2146-15	BOLD:ACE7299	BIOUG22342-F11	591[0n]	Canada	British Columbia	Meeting of the Waters Trail
Phlaeopterus lagrandeuri	UAMIC632-13	BOLD:ACE7299	UAM:Ento:203074	407[0n]	United States	Alaska	PoW Is. Luck Lk. Rd. 1
Phlaeopterus lagrandeuri	UAMIC633-13	BOLD:ACE7299	UAM:Ento:203075	658[0n]	United States	Alaska	PoW Is. Luck Lk. Rd. 1
Phlaeopterus loganensis	BBCCN358-10	BOLD:AAP7088	10PCCOL-0263	658[0n]	Canada	Alberta	
Phlaeopterus longipennis	PHLA065-20	BOLD:AEE6165	UAMObs:Ento:234973	653[0n]	United States	Oregon	Clackamas County, Mt. Hood Nat. Forest, Still Creek trib. at HWY 173
Phlaeopterus longipennis	PHLA066-20	BOLD:AEE6165	UAMObs:Ento:234974	627[0n]	United States	Oregon	Clackamas County, Mt. Hood Nat. Forest, Still Creek trib. at HWY 173
Unamis columbiensis	CNRVG2712-15	BOLD:ACT9387	BIOUG20368-D06	658[0n]	Canada	British Columbia	
Unamis sp.	UAMIC2297-14	BOLD:ACS3291	UAM:Ento:152313	575[2n]	United States	Alaska	Juneau, Heintzleman Ridge
Unamis sp.	UAMIC2351-14	BOLD:ACS3291	UAM:Ento:152315	579[0n]	United States	Alaska	Juneau, Heintzleman Ridge
Unamis sp.	UAMIC2352-14	BOLD:ACS3291	UAM:Ento:152316	568[0n]	United States	Alaska	Juneau, Heintzleman Ridge

2.2.1. List of morphological characters

Character descriptions follow for our morphological data. All characters are unordered and equally weighted. Figures are primarily from Mullen et al. (2018), cited below as "fig. M#" or "figs M#,#" using a capital M to distinguish them from figures herein, cited as Fig. #.

1. Maximum size: (Figs 1, 2) (**0**) less than 5.0 mm; (**1**) greater than 6 mm. This character represents J.M. Campbell's hypothesis that the large-bodied species form a monophyletic group. In Figs 2, 4–7, the large-bodied species, corresponding to state 1, are colored red, blue, or green.

2. Maximum size: (Figs 1, 2) (**0**) less than 7.8 mm; (**1**) greater than 8.1 mm. Character one and two reflect the hypothesis that the largest bodied species with maximum lengths over 8.1 mm are a clade within or sister to the large-bodied species that are over 6 mm in length. Because small body size is plesiomorphic, characters one and two do not represent double-weighting of small body size. In Figs 2, 4–7, the largest bodied species, corresponding to state 1, are colored blue.

3. Body length to width ratio: (**0**) wide, length to width ratio under 3 (figs M1, 2B–D, 3A, C, D, 4, 5); (**1**) elongate, length to width ratio greater than 3 (figs M2A, 3B).

4. Ocelli: (**0**) present (figs M34A–D, 35A–D); (**1**) absent (fig. M34E, F).

5. Color of elytra: (**0**) dark brown, light brown, or dark reddish brown, to black (figs M2, 4); (**1**) light reddish to yellowish brown (figs M1B, 3C); (**2**) bicolored, part dark to light brown, part yellowish to reddish yellow (fig. M3D).

6. Antocellar foveae (dorsal impressions between eyes) shape: (**0**) elongate narrow (fig. M27); (**1**) elongate wide (figs M34C–F); (**2**) oval to circular (figs M35A–D); (**3**) reduced (fig. M34A, B).

7. Nuchal constriction: (**0**) distinct, post-ocular region clearly divided into temple and neck with impression continuing across midline of neck (fig. M27); (**1**) vague (figs M34A, B, 35A–D; (**2**) absent (fig. M34C–F).

8. Interantennal impression: (**0**) present (fig. M35A–D); (**1**) obsolete. This is a transverse impression that runs across the frons between the bases of the antennae.

9. Interfacetal setae of eye: (**0**) present on most of eye (often glabrous in extreme dorsal portion) (fig. M35E, F); (**1**) absent from most of eye (glabrous in dorsal half, reduced in number or glabrous on ventral half) (fig. M36A–F).

10. Shape of labrum: (**0**) 0.3–0.5 times as long as wide (fig. M31A, B, E, F); (**1**) less than 0.3 times as long as wide (fig. M31C, D).

11. Dorsal surface of labrum: (**0**) without micropores (fig. M31A); (**1**) with micropores limited to setose region (fig. M31B–G); (**2**) with micropores across labrum, many posterior to setose region (fig. M31H).

12. Minimum width of gula: (**0**) narrow, less than 0.2 times as wide as mentum (fig. M41E, F); (**1**) wide, more than 0.2 times as wide as mentum (fig. M42).

13. Base of epipharynx: (**0**) with oblique, parallel rows of fine ridges (fig. M33A–D); (**1**) without rows of ridges (fig. M33E–H).

14. Apical portion of epipharynx: (**0**) with spines extending to apical margin (fig. M33A, B, E–H); (**1**) smooth (fig. M33C, D).

15. Center of epipharynx: (**0**) with many widely spaced large spines (fig. M33A, B); (**1**) with many closely spaced small spines (fig. M33C–H).

16. Maxillary palpi (length of fourth vs. third palpomere): (**0**) apical palpomere on average at least 3.5 times as long as third (figs M30E, 32A); (**1**) apical palpomere on average 3 to 2.55 times as long as third (fig. M32B, C); (**2**) apical palpomere on average less than 2.47 times as long as third (fig. M32D). Five specimens of each species (except *P. czerskyi* – we only had two) were measured which revealed an inverse relationship between a species' average 4th vs 3rd maxillary palpomere ratio and increasing body length ($R^2 = 0.5742$, $p = 0.00027$). States were chosen to correspond to breaks in the data. Larger bodied *Phlaeopterus* have 3rd palpomeres considerably longer than smaller bodied species, relative to the length of their 4th palpomeres.

17. Fine cilia at base of hypopharynx: (**0**) in oblique rows (fig. M40A, B); (**1**) not in rows (figs M40C–F, 41A–C).

18. Micropits of antennae: (**0**) present and with numerous non-protruding papilliform structures (fig. M37B–E); (**1**) absent or reduced to tiny pits (fig. M37A); (**2**) present and with pore-like openings (fig. M37H, I); (**3**) present and with numerous protruding papilliform structures (fig. M37F, G, J, K).

19. Molar area of mandible: (**0**) with fine parallel rows of short setae or setiform projections (fig. M28A, B); (**1**) with no setae or setiform projections (fig. M28C–F, 29A–C). It is unknown if these structures are true setae or setiform projections.

20. Prosthecal fringe of mandible: (**0**) does not extend apicad of the subapical mandibular tooth (fig. M28A, B); (**1**) extends beyond subapical mandibular tooth (figs M28C–F, 29A–C).

21. Mesal margin of mandible: (**0**) not curved, angulate, or excavate apicad of the molar area (fig. M28A–D); (**1**) curved, angulate, or excavate apicad of the molar area (figs M28E, F, 29A–C).

22. Lateral area of pronotum: (**0**) with no, or only trace of impression (fig. M15A, B); (**1**) moderately impressed (figs M15C–H, 17E); (**2**) deeply impressed, foveiform (fig. M16).

23. Base of pronotal disk: (**0**) without pair of transverse shallow impressions (figs M15, 16, 17A, B, E); (**1**) with pair of transverse shallow, sometimes confluent, impressions (fig. M17C, D).

24. Pronotal width to head width: (**0**) less than 1.5 (figs M2A, B, 3A, B, D, 4B, C); (**1**) more than 1.55 (figs M1A–C, 2C, D, 3C, 4A, D 5A, B).

25. Pronotal lateral margins posterior to lateral impressions: (**0**) not deflexed (figs M15C–E, 16, 17A, B); (**1**) deflexed posterior to deeply impressed lateral impressions (fig. M17C, D); (**2**) deflexed posterior to obsolete or vaguely impressed lateral impressions (figs M15F–H, 17E).

26. Anterior ridge of mesoventrite: (**0**) with no projection or only a small median posterior lobe (figs M19A–D, 20F); (**1**) prolonged posteriorly into a long projecting median tooth (figs M19E, F, 20A–E).

27. Second tooth posterior to first on midline of mesoventrite: (**0**) absent (fig. M19E); (**1**) present (fig. M20E). Those without a first tooth also lacked a second tooth so were coded inapplicable for this character. This second tooth is easily seen in a lateral view of most specimens that have been card mounted.

28. Mesoventral carina: (**0**) present along midline (figs M19A–D, 20E); (**1**) vague or absent (figs M19E, F, 20A, B, F).

29. Apical margin of elytra: (**0**) convex or subtruncate (figs M1, 2A, C, D, 3, 4B–D, 29F); (**1**) prolonged at suture only in females (figs M2B, 29G); (**2**) prolonged at suture in both sexes (figs M4A, 29E).

30. Metathoracic wings: (**0**) fully developed; (**1**) reduced or absent; (**2**) fully developed in most individuals but reduced in some.

31. Glabrous portion of mesotibia: (**0**) absent; (**1**) present (fig. M18).

32. Apical tooth on metatrochanter: (**0**) absent; (**1**) present (fig. M41D).

33. Humeral angles of elytra: (**0**) convex, epipleural carina not projecting (figs M1B–D, 2–5); (**1**) more rectangular, epipleural carina projecting and explanate (fig. M1A).

34. Shape of wing-folding spicule patches on tergite 5: (**0**) round and widely separated; (**1**) broadly oval and narrowly separated or so close as to appear combined into a single transverse band (fig. M17F–H); (**2**) absent. The presence of these spicules is logically correlated with the presence of wings, and indeed, *P. czerskyi* is brachypterous and lacks these spicules, however, *P. houkae* is brachypterous and has these spicules.

35. First metatarsomere: (**0**) shorter than ultimate tarsomere; (**1**) subequal to or longer than ultimate tarsomere (figs M1–5).

36. Paramere length to median lobe length ratio: (**0**) 1.16 or less (figs M21B–F, 22, 23, 24, 26); (**1**) 1.19 or greater (figs M21A, B, 25B, D). Measurements were taken from the figures in Mullen et al. (2018) with averages used for species with multiple figures except the subspecies of *P. castaneus*, which were not averaged. Measurements were taken from the median junction of the parameres to the paramere and median lobe apices.

37. Internal sac shape (inverted): (**0**) not rectangular (figs M21, 22, 23, 24A, B, 25B–D); (**1**) rectangular wide (figs M24D, 25A); (**2**) rectangular elongate (fig. M24C).

38. Carina of median lobe apex: (**0**) absent (figs M21A–D, 22B–D, 23, 24A, C, D, 25, 26); (**1**) present (figs M21E, F, 22A, 24 B).

39. Internal sac spinature: (**0**) few to no microspinules; (**1**) sclerites and many sparse microspinules (fig. M21A–D); (**2**) covered with microspinules (figs M21E, F, 22–26).

40. Internal sac microspinule pattern: (**0**) not denser basally (figs M21, 22, 23B–D, 24A, C, D, 25, 26); (**1**) denser basally (figs M23A, 24B). Those with few to no microspinules were coded inapplicable for this character.

2.3. Molecular data

Our molecular dataset contains 164 partial sequences of the mitochondrial gene cytochrome c oxidase subunit 1 (COI), representing nine *Phlaeopterus* species, six *Lesteva* species, and one *Unamis* species (Table 2). We sequenced COI fragments from previously unsequenced specimens and added 107 public sequences from BOLD after filtering out sequences less than 400 bp in length, those flagged as possible misidentifications or contaminations, those with 5 or more ambiguous character states, and those with stop codons. These included data from Hendrich et al. (2015), Pentinsaari et al. (2014), and Sikes et al. (2017). We also included one non-public sequence for *Phlaeopterus loganensis* provided to us with permission by the Canadian National Collection of Insects, Arachnids and Nematodes (CNC), Ottawa, Ontario, Canada (Table 2).

Sequences ranged from 403 to 654 bp in length. We extracted DNA from whole hind legs using Qiagen DNeasy extraction kits following the "Purification of Total DNA from Animal Tissues" protocol in the DNeasy Blood and Tissue Handbook that came with the extraction kit. We amplified a 658-bp region of COI using standard COI barcoding forward and reverse primers, LCO-1490 and HCO-2198, respectively (Folmer et al. 1994). We ran all PCR reactions at 25-µl volume. Typical PCR reaction solution included: 12.5 µl GoTaq Green Master Mix, 1.0 µl forward primer, 1.0 µl reverse primer, 8.5 µl H_2O, and 2.0 µl template DNA. We used the thermocycler protocols of Folmer et al. (1994) except where noted. Typical thermocycler protocol included a single cycle of 95°C followed by 35 cycles of 95°C for 30 seconds of denaturation, 45°C for one minute of annealing, and 72°C for two minutes of elongation, followed by a single extension of 72°C for 10 minutes.

We viewed sequence data with 4Peaks (Griekspoor and Groothuis 2005) and aligned sequences by eye in MacClade 4.08 and Mesquite 3.6 (Maddison and Maddison 2005, 2016). We created consensus sequences from bidirectional reads, aligned by eye, then checked our alignment by translation to amino acids and alignment by amino acid codon position using the "minimize stop codons" option in Mesquite to find the reading frame. The final alignment was free of stop codons and aligned with a published *Lesteva longoelytrata* (Goeze,

1777) COI sequence (GenBank accession: KM442270.1, Hendrich et al. 2015) in both nucleotide and amino acid alignment. Voucher specimens used for DNA extractions can be found in the following insect collections: University of Alaska Museum (UAM), Canadian National Collection of Insects (CNC), California Academy of Sciences (CAS), Santa Barbara Museum of Natural History (SBMNH), Field Museum of Natural History (FMNH), Smithsonian Museum of Natural History (NMNH), University of Idaho William F. Barr Entomological Museum (WFBM), and Brigham Young University Monte L. Bean Life Science Museum (BYUC). Digital records of specimen collection data we used to generate new sequences are available through the UAM Arctos database (https://arctos.database.museum/saved/PhlaeopterusBold). Our molecular data matrix and trees are archived at http://purl.org/phylo/treebase/phylows/study/TB2:S27393 and as Supplementary files S1, S2, and S3. GenBank and BOLD accession / process ID numbers for our sequence data are provided in Table 2.

2.4. Phylogenetic Analysis

2.4.1. Model selection

We used PartitionFinder 2.1.1 on the CIPRES Science Gateway (Guindon et al. 2010; Miller et al. 2010; Lanfear et al. 2016) with the more thorough, non-greedy search algorithm to choose a partitioning scheme and model of sequence evolution using the AICc. The best partitioning scheme for the COI dataset was by codon position with the 1st positions best fit by the TRN+G model, the 2nd positions best fit by the TIM+I model, and the 3rd positions best fit by the GTR+G model. We used these models for our ML analysis in GARLI (see section 2.4.3. below). For MrBayes, which lacks the first two models, PartitionFinder recommended use of GTR+G for the 1st and 3rd positions and GTR+I+G for the 2nd positions.

We used Bayes factors (Kass and Raftery 1995) to determine if gamma correction for among-character rate heterogeneity was warranted for the Mkv model (Lewis 2001) used for the morphological data. We compared the performance of the two models, Mkv with or without gamma distribution, using a stepping stone (SS) analysis in MrBayes v3.2 (Xie et al. 2011) with the search parameters described in section 2.4.2 below, with the exception of the number of steps of the MCMC chain, which was increased 10-fold as recommended in the MrBayes manual (Ronquist et al. 2020), and the default values for the SS command. A SS analysis yields more accurate marginalized likelihood scores than the harmonic mean and is thus preferred for use in Bayes factors tests (Xie et al. 2011). However, all other values from a SS analysis, including the topology and posterior probabilities, should be ignored because they are not derived from the posterior distribution (P. Lewis, pers. comm). All SS analyses resulted in 50 steps with 1960000 generations (1960 samples) within each step. As indicated in the MrBayes v3.2 manual (Ronquist et al. 2020), $2 \times \log_e$ Bayes factors interpretation for a MrBayes analysis proceeds as follows: values of less than 2 indicates weak to no evidence for the better model, 2–6 indicates positive evidence, 6–10 indicates strong evidence, and greater than 10 indicates very strong evidence for the better model (Kass and Raftery 1995). There was considerable variance in the marginalized likelihoods of the paired SS runs of the morphological data with and without gamma. This might result from the small number of parsimony informative characters in the morphological data (35) relative to the number of parameters being estimated, including branch lengths (46). The likelihoods of the paired runs without gamma were –18.69 and –108.93 with a mean of –19.38, and with gamma were –110.85 and –20.45 with a mean of –21.15. The Mkv model without gamma was 1.77 log-likelihood units better (a Bayes factor of 3.54), so the Mkv model without gamma distribution was used. We used the Mkv model rather than the parsimony model because the Mkv model is statistically consistent and has been shown to outperform parsimony for commonly encountered types of morphological data (Wright and Hillis 2014).

2.4.2. Bayesian phylogenetic analyses

We performed all Bayesian analyses using MrBayes 3.2.7a x86_64 (Ronquist et al. 2012) without the BEAGLE option on the CIPRES Science Gateway (Miller et al. 2010). We ran each analysis (concatenated, COI only, morphology only) using two simultaneous Metropolis-coupled Markov chain Monte Carlo runs of 4 chains for 10,000,000 steps with default priors and sampled every 1,000 generations resulting in 20,002 trees sampled. We discarded the first 25% resulting in 15,002 post burn-in trees. To determine if stationarity had been reached, we used the following criteria: 1) split frequencies less than or equal to 0.01; 2) effective sample size (ESS) greater than 100 for all parameters; and 3) Potential Scale Reduction Factor equal to 1.0. All runs reached stationarity based on these criteria. We consider estimated posterior probabilities (PP) ≥ 0.95 to constitute strong branch support, with values ≥ 0.75 and < 0.95 to constitute moderate branch support.

2.4.3. Maximum Likelihood phylogenetic analyses

We performed maximum likelihood bootstrapping (MLBS) for each analysis (concatenated, COI only, morphology only) using Garli 2.01 (Zwickl 2006) on the CIPRES Science Gateway v3.3 (Miller et al. 2010). We partitioned the data by codon position with morphology as the 4th partition, and used the models described above (section 2.4.1). We assembled a 50% majority rule consensus tree of the resulting 200 bootstrap replicates using PAUP 4.0a build 167 (Swofford 2002) and added these values to the consensus phylograms that resulted from the Bayesian analyses. We consider bootstrap values ≥ 75 to constitute strong branch support, with values ≥ 50 and < 75 to constitute moderate branch support.

2.4.4. Concatenated analysis

Our concatenated analyses were performed after merging all COI sequences within each species using Mesquite 3.6 (Maddison and Maddison 2016). Sequences not identified to species were not included. This merging process produces maximally complete sequences for each species and retains all the polymorphisms within each species. The COI data were then combined in a single Nexus file with the morphological data and analyzed using MrBayes and Garli as a partitioned analysis with a separate model for each codon position of COI and the Mkv model for the morphological data, as described above.

2.5. Hypothesis testing

We tested the monophyly of prior taxonomic hypotheses, as well as unpublished taxonomic groupings (Table 1) using estimated posterior probability (PP) support values obtained from our Bayesian analyses. Taxon relationships that did not occur in any of the sampled trees in an MCMC run were assumed to have a PP of < 1/number of trees sampled (Miller et al. 2002; Holder and Lewis 2003). In our analyses, such clades have a PP < 0.0001. Of particular interest was the unpublished hypothesis of Campbell '*Phlaeopterus* sensu stricto' which states that all the large-bodied species are descended from a large-bodied common ancestor, i.e. large body size evolved once in the genus.

To provide an additional test for this hypothesis, we used Bayes factors (Kass and Raftery 1995; Ronquist et al. 2020) to compare the means of the marginalized likelihood scores of two stepping stone MrBayes (Xie et al. 2011) analyses, one with a topological partial constraint enforced that required all large-bodied species except *P. bakerensis*, which was free to join anywhere, to form a clade, and one with a partial constraint that required all large-bodied species except *P. elongatus* Mullen and Campbell, 2018, which was free to join anywhere, to form a clade (the constrained clade had 12 taxa in both cases). This approach includes one analysis forcing *P. elongatus* to belong to the clade of large-bodied species and one allowing *P. elongatus* to join anywhere but keeps the size of the clade the same in both analyses. For the COI data, we balanced the topological constraint so that there were 84 constrained sequences in both analyses. Comparing two analyses with the same number of constrained taxa eliminates the differences in the topology priors that would result from comparing a constrained to an unconstrained analysis, or to a constrained analysis with a different number of constrained taxa. Bergsten et al. (2013) documented the important influence of topology priors on Bayes factors tests of analyses with topological constraints, and ways to improve the reliability of these tests. Stepping stone runs with the morphology-only data resulted in high variance among estimated marginal likelihood scores that inexplicably fell into three bins (scores 109–112, 235–238, and 380–383). Although the results from the morphology-only Bayes factor comparisons, within bins, agreed with the conclusions found from the concatenated and COI analyses, this high variance led us to doubt the reliability of the morphology-only Bayes factors results so they are not shown.

To test an alternative hypothesis that the most recent common ancestor of the genus *Phlaeopterus* was large-bodied with subsequent reversals to small-bodied adults in some species, we performed ancestral character state reconstruction with Mesquite 3.6 (Maddison and Maddison 2016) to estimate the body size of the most recent common ancestor of the genus using the Mk1 model, the morphology only matrix, and the concatenated analysis tree (Fig. 4). We also explored an asymmetric two-parameter likelihood model and a step matrix parsimony model to see what ratio of gains to losses would be needed to estimate the common ancestor as large-bodied (Cunningham et al. 1998). A likelihood ratio test performed in Mesquite rejected the asymmetric two parameter model as overfitting the data (Chi-square, p = 0.9233) so we present only the results under the one parameter model. We tested the monophyly of *Phlaeopterus* species using the full 164-sequence COI dataset.

If a monotypic genus concept failed to match our trees due to paraphyly resulting from the missing species being unknown at the time the genus was erected, such as Motschulsky's (1853) original concept for *Phlaeopterus*, we considered the concept untestable. Casey's (1893) concept of *Phlaeopterus* being a junior synonym of *Tilea* and Scheerpeltz's (1933) reversal to make *Tilea* a junior synonym of *Phlaeopterus* (in accordance with the principle of priority) we considered untestable using phylogenetics because neither of these concepts makes phylogenetic predictions. However, Fauvel's (1878) erection of *Tilea* as a monotypic genus for *P. cavicollis* Fauvel, 1878 could be tested because, following current classification practices, it predicts this species would fall outside the clade containing the rest of the *Phlaeopterus* species. The same is true for Casey's (1885) erection of the monotypic genus *Vellica* for *P. longipennis* Casey, 1885. However, all hypotheses relating to the monophyly and generic status of *Phlaeopterus* are only weakly testable given our taxon sampling. To strongly test these would require much denser sampling within *Lesteva*, *Unamis* and other anthophagine genera to test the monophyly of genera relative to all of the genera within the tribe.

All the large-bodied species are reported as snowfield-associated, and two of the small-bodied species are also (*P. lagrandeuri* and *P. houkae* Hatch, 1957). To determine if there is a relationship between body size and use of snowfields as habitats, one additional character representing habitat was added to conduct a character correlation analysis, also known as a test of independent evolution, using Pagel's (1994) method as implemented in Mesquite 3.6 (Maddison and Maddison 2016). The habitat character was binary: (0) not snowfield associated; (1) snowfield associated, and was not used in the phylogenetic inference. The topology from the concatenated analysis was used with the option to seek any relationship (i.e. any effect of X on Y or Y on X) between character 1 (maximum body size) and this binary habitat

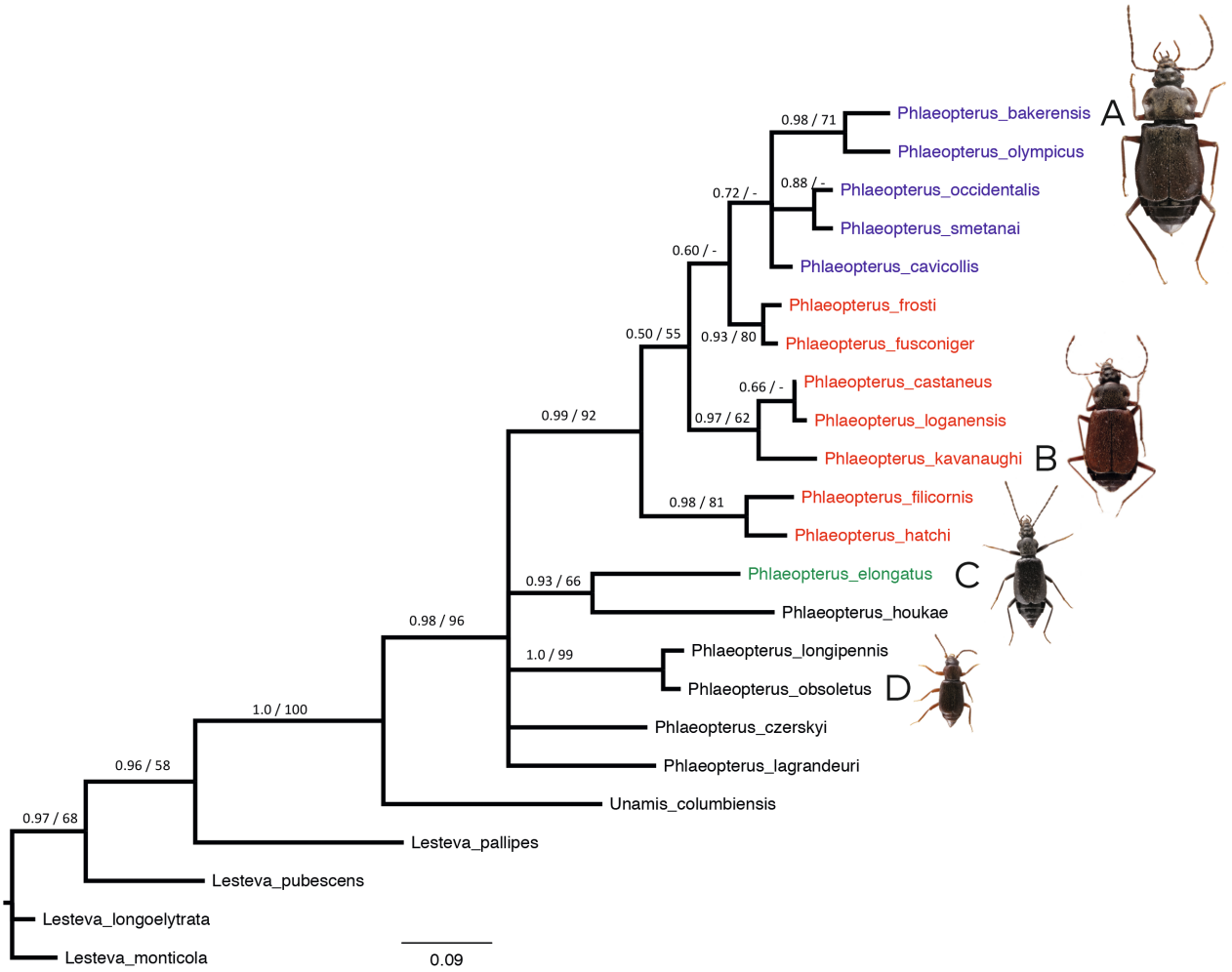

Figure 4. Evidence that large body size evolved twice: a clade of large bodied species (red and blue colors) and a separate origination of large body size in *P. elongatus* (green). Concatenated Bayesian analysis of 40 morphological characters and 404–654 bp of COI with posterior probability and maximum likelihood bootstrap support values near each branch with 18 *Phlaeopterus* ingroup species, 1 *Unamis* and 4 *Lesteva* outgroup species. Topology is a Bayesian 50% majority rule consensus phylogram. Clades with ML bootstrap values less than 50% are indicated with a "–". Taxon names in blue and red are species with maximum body sizes over 6.5 mm. Blue indicates the largest species, those with maximum sizes over 8 mm, illustrated by A) *P. bakerensis*; names in red are species with maximum body sizes 6.5 to 7.9 mm with wide bodies, illustrated by B) *P. kavanaughi*; the name in green is for C) *P. elongatus* with a maximum body size of 6.4 mm, with an elongate body; names in black are species with maximum body sizes below 5 mm, illustrated by D) *P. obsoletus*. Beetle inset illustrations are scaled to approximate relative body sizes.

character, with 1000 simulations to estimate the p-value. Habitat data were taken from Mullen et al. (2018) and specimen label data. This test compares the likelihoods of a four-parameter model to an eight-parameter model (we used ten iterations per simulation).

3. Results

3.1. Sequence statistics

Our COI alignment is 654 bp long and comprises 164 sequences including the outgroup taxa (113 ingroup sequences). Base composition is as follows: A = 29.5%, C = 17.63%, G = 16.44%, T = 36.42%. These values are within the range typically reported for insect mitochondrial DNA (Dowton and Austin 1997). Our full COI dataset contains 216 parsimony-informative sites and 425 constant sites, with 81% (n = 175) of the parsimony informative sites found in the 3rd codon position. The Chi-square test of homogeneity of base frequencies across taxa as implemented in PAUP* 4.0 resulted in a Chi-square value = 182.0 (df = 489) with a p-value = 1.0, suggesting that nucleotide frequencies across taxa were stationary.

When *P. loganensis* is removed from our data, uncorrected p-distances within and among *Phlaeopterus* species' COI sequences are above 4% for among-species comparisons (min 4.23%, mean 10.52%, max 14.96%) and below 4% for within-species comparisons (min 0.00%, mean 0.53%, max 3.08%). *Phlaeopterus castaneus* has a minimum among-species distance of 0% with *P. loganensis*, and is also the only species with within-species distances above 2.08% (8 of 15 within-species comparisons for this species had distances ranging from 2.29 to 3.08%).

3.2. Concatenated phylogeny

Our most inclusive estimate of the phylogeny of *Phlaeopterus* resulted from the concatenated COI+morphology data (Fig. 4). The genus *Phlaeopterus* is well supported as monophyletic (PP = 0.98, MLBS = 96). A clade with 12 large-bodied species is well supported (PP = 0.99, MLBS = 92) but emerges from a four-branch polytomy of smaller-bodied species, including the large-bodied *P. elongatus* – indicating that large-bodied adults evolved twice in the genus. Within the clade of large-bodied species is nested a clade of the largest-bodied *Phlaeopterus* (maximum body size over 8 mm). This clade was weakly supported in the Bayesian analysis (PP = 0.72), but not supported in the maximum likelihood bootstrap analysis (MLBS < 50).

3.3. Molecular phylogeny

A 50% majority rule consensus tree resulting from Bayesian analysis of the COI dataset is shown in Fig. 5. This tree is better resolved than the combined COI+morphology phylogeny (Fig. 4), although the backbone has some weak branch support with posterior probabilities in the 0.70s and maximum likelihood bootstrap values < 50. This phylogeny differs from the combined COI+morphology and morphology-only phylogenies in the placement of the small-bodied *P. lagrandeuri* and the large-bodied *P. elongatus* as sister species with high Bayesian support (PP = 0.96) but weak ML bootstrap support (MLBS = 57).

This phylogeny supports the monophyly of seven of the nine *Phlaeopterus* species in the analysis with strong posterior probabilities (all PP > 0.98) but mixed strong to weaker maximum likelihood bootstrap support (MLBS 67–100). However, the two *P. loganensis* sequences nest within a clade of *P. castaneus* sequences. *Phlaeopterus castaneus* is one of two ingroup species with multiple well-supported clades separated by relatively long branches, the other being *P. fusconiger*.

3.4. Morphological phylogeny

The 50% majority rule consensus tree of the morphology dataset (Fig. 6) contains one well supported large clade of large-bodied species that is nested within a three-branch polytomy of small-bodied species. The basal polytomy includes all the small-bodied *Phlaeopterus* species (maximum body size less than 5 mm, 5 species) and also includes the large-bodied *P. elongatus*. The larger, well supported clade (PP = 0.99, MLBS = 88) includes all the large-bodied *Phlaeopterus* species (maximum body size more than 5 mm, 12 species) except *P. elongatus*. Body lengths for all *Phlaeopterus* species are shown in Fig. 2.

3.5. Hypothesis testing

A summary of Bayesian PP support for taxonomic hypotheses of *Phlaeopterus* in the COI+morphology (Fig. 4), COI-only (Fig. 5), and morphology-only (Fig. 6) phylogenies is given in Table 3. All three analyses strongly rejected Fauvel's (1878) and Casey's (1885) hypotheses suggesting *P. cavicollis* and *P. longipennis* were lineages separate from *Phlaeopterus* deserving of generic rank status (Tables 1, 3). Of the unpublished species group hypotheses, all but two that could be tested were strongly rejected as polyphyletic or paraphyletic, including the '*Phlaeopterus* sensu stricto' hypothesis that all the large-bodied species descended from a common large-bodied ancestor (Figs 4–6).

The stepping stone Bayes factor analyses using partial constraints, one forcing *P. elongatus* to belong to the clade of large-bodied species and one allowing *P. elongatus* to join anywhere, found strong to very strong evidence for large body size evolving twice in the genus (Table 4). Analyses that forced *P. elongatus* to join the clade of large-bodied species were significantly worse than those that did not. This result agrees with the strong posterior probabilities for the two branches separating *P. elongatus* from the clade of large-bodied species in the COI analysis (PP = 0.91 and 1.0, Fig. 5).

Ancestral character state reconstruction of character one, using the morphology only matrix and the tree in Fig. 4, under the Mk1 model, estimated the most recent common ancestor of *Phlaeopterus* as small-bodied with a proportional likelihood of 0.9978. Under a step matrix parsimony model for character one, the cost of evolving a large body size would have to be 2.6 times or more than the cost of evolving a small body size to estimate the common ancestor of the genus as large-bodied.

Campbell's unpublished hypotheses for the *longipennis* species group, which suggested a sister species relationship between the only two species in the genus without ocelli, was strongly supported in the COI+morphology and morphology analyses (Table 3) but was untestable in the COI-only analysis in the absence of DNA sequence for *P. obsoletus* Mullen and Campbell, 2018. The unpublished hypothesis for the *castaneus* species group (*P. castaneus* and *P. kavanaughi* Mullen and Campbell, 2018, as sister species) was strongly supported in the morphology-only analysis but rejected in the other two analyses because *P. loganensis* was intermixed with the clade of *P. castaneus* sequences in the majority of sampled trees (Table 3, Fig. 5). However, the concatenated analysis did not reject this hypothesis strongly – fully one third of the post-burnin MCMC trees included *P. castaneus* and *P. kavanaughi* as sister taxa (Table 3).

The character correlation test to determine if character 1 (maximum body size) is correlated with the use of snowfields as a habitat failed to reject the null hypothesis of independence (p-value = 0.06), albeit weakly.

4. Discussion

Here we present a preliminary phylogeny of the genus *Phlaeopterus*, using both morphological and molecular data. These analyses were used to test previous taxo-

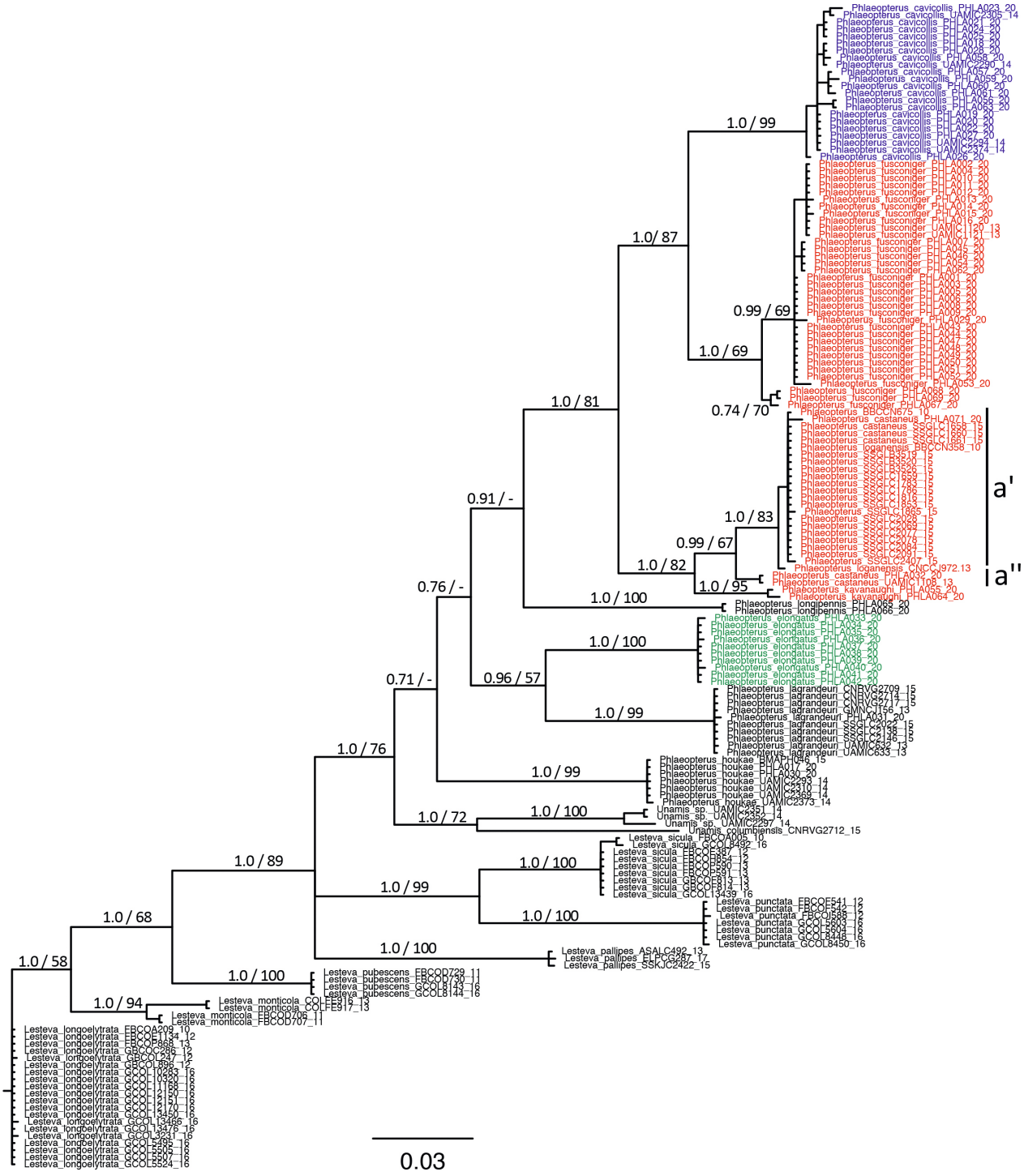

Figure 5. Bayesian analysis of 164 sequences, 404–654 bp in length, of the mitochondrial gene COI with posterior probabilities and Garli maximum likelihood bootstrap values above each branch. Included are 9 *Phlaeopterus* ingroup species and 1 *Unamis* and 6 *Lesteva* outgroup species Topology is a Bayesian 50% majority rule consensus phylogram. One intermixed clade of the species *P. castaneus* + *P. loganensis* is indicated at (a), with (a') indicating the subspecies *P. castaneus castaneus* and (a'') indicating the subspecies *P. castaneus cascadiensis*. Taxon names in blue are species with maximum body sizes over 8 mm; names in red are species with maximum body sizes 6.5 to 7.9 mm with wide bodies; names in black are species with maximum body sizes below 5 mm; the name in green is for *P. elongatus* with a maximum body size of 6.4 mm, with an elongate body.

nomic hypotheses of the genus (Table 3), as well as the monophyly of *Phlaeopterus* species (Figs 4–6). We found strong support for the recent synonymization of *Vellica* under *Phlaeopterus* (Figs 4–6, Table 3) that was performed in Mullen et al. (2018). This agrees with Newton et al. (2000) who suggested that *Vellica* was likely not distinct from *Phlaeopterus*. The only two morphology-based hypotheses that received strong support (*longipennis* and *castaneus* species groups) were those whose support came entirely from the morphological data (Table 3). There were none that received strong support from the COI-only data, although this was in part a result of the

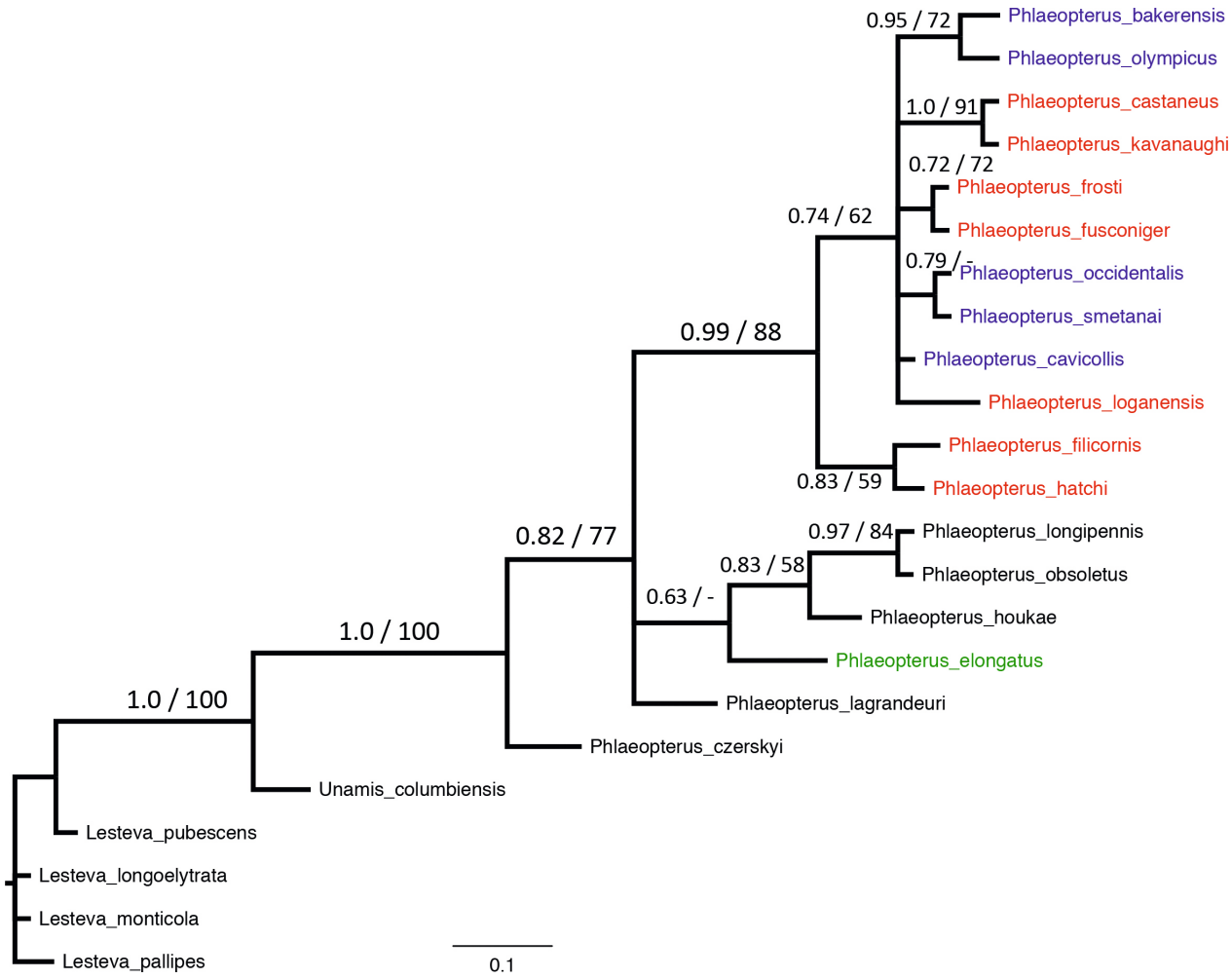

Figure 6. Bayesian analysis of 40 morphological characters with posterior probabilities and Garli maximum likelihood bootstrap values near each branch with 18 *Phlaeopterus* species and 1 *Unamis* and 4 *Lesteva* outgroup species. Topology is a Bayesian 50% majority rule consensus phylogram. Taxon names in blue are species with maximum body sizes over 8 mm; names in red are species with maximum body sizes 6.5 to 7.9 mm with wide bodies; names in black are species with maximum body sizes below 5 mm; the name in green is for *P. elongatus* with a maximum body size of 6.4 mm, with an elongate body.

lack of DNA data for various taxa, which prevented some hypotheses from being tested.

The concatenated COI+morphology phylogeny (Fig. 4) is more comprehensive than the COI-only (Fig. 5) or morphology-only (Fig. 6) phylogenies because it incorporates evidence from morphology, which is encoded by the nuclear genome, and mitochondrial DNA data, and includes nine species for which we lacked molecular data. We feel that despite the polytomies in our concatenated phylogenetic estimate, it is currently the best estimate of evolution in the genus *Phlaeopterus*.

Although our results are preliminary and not all strongly supported, some inferences can be made. Our phylogenetic and Bayes factors analyses suggest there were two separate evolutionary changes towards maximum body sizes greater than 5 mm, once in *P. elongatus*, and once in the common ancestor to the other large-bodied species (Figs 4–6), with a further body size increase in the clade of the largest species.

Our maximum likelihood ancestral character state reconstructions estimated the common ancestor of the genus as small-bodied with high probability (99%), thus rejecting a hypothesis that the ancestor was large-bodied with subsequent reversals to small body size. The outgroup *Lesteva* and *Unamis* species in our study, and all the newly transferred and described *Phlaeopterus* from Asia, are small-bodied (Fig. 2) (Shavrin 2020), as are most anthophagines, reinforcing our conclusion that the common ancestor of *Phlaeopterus* was small-bodied.

Under a step matrix parsimony model the evolution of large body size would have to cost 2.6 or more times than the evolution of small body size to infer the common ancestor as large-bodied. This would make the large-bodied species a paraphyletic group with three to four changes to small-bodied adults within the genus. However, this hypothesis does not correspond with Campbell's original idea that the common ancestor of the genus was small-bodied with the large-bodied species forming a monophyletic subgroup of the genus. Nevertheless, it is an alternative scenario that would explain the evolution of body size in the genus but is less parsimonious than assuming equal state change costs. In contrast to investigations of wing loss in insects, where there are abundant data indicating wing loss is far more common than wing

Table 3. Tests of taxonomic hypotheses of the genus *Phlaeopterus*. g = genus, sg = informal species group.

Hypothesis	Posterior probability morphology + COI	Posterior probability COI	Posterior probability morphology
Tilea g	<0.0001	<0.0001	<0.0001
Vellica g	<0.0001	<0.0001	<0.0001
longipennis sg	1.0	-	0.97
castaneus sg	0.3316	<0.0001	1.0
cavicollis sg	<0.0001	-	<0.0001
fusconiger sg	<0.0001	<0.0001	<0.0001
filicornis sg	<0.0001	-	<0.0001
Phlaeopterus sensu stricto	<0.0001	<0.0001	<0.0001

Table 4. Results of MrBayes stepping stone Bayes factor analyses showing the estimated marginal likelihoods of two independent runs, their means, the difference (under the better hypothesis – that of *P. elongatus* not being in the clade of large-bodied species), Bayes factors, and strength of evidence in support of the better hypothesis. Outlier values are in italics.

independent MrBayes run	concatenated, clade with *P. elongatus*	concatenated, clade without *P. elongatus*	COI, clade with *P. elongatus*	COI, clade without *P. elongatus*
run 1	–3174.19	–3168.02	*–4949.97*	–4951.03
run 2	–3174.20	–3167.91	–4958.05	–4952.34
run 3	–3174.28	–3167.95	–4955.61	–4949.75
run 4	*–3155.20*	–3167.87	–4962.54	–4948.60
run 5	–3174.19	–3168.01	–4957.85	–4946.45
run 6	–3174.08	–3167.96	–4953.79	–4949.58
mean	–3171.02	–3167.95	–4956.30	–4949.63
difference		3.07		6.67
Bayes factor		6.14		13.34
Strength of evidence for better hypothesis		strong		very strong

Note: Run 4 of concatenated with *P. elongatus* is a significant outlier, if excluded the BF doubles & evidence = very strong

gain (Whiting et al. 2003; Stone and French 2003), we can think of no theoretical or biological justification for use of these unequal costs in this case. That is, there is no reason to believe it is harder for these beetles to become large-bodied than small-bodied. There are 13 large-bodied species (> 5 mm) in the genus, nine small-bodied, and no evidence of a small-bodied species evolving from large-bodied ancestors, which if suggestive at all (ignoring phylogenetic inertia), indicates large bodies may be easier to acquire and maintain than small bodies in *Phlaeopterus*.

It is interesting that of the eight small-bodied *Phlaeopterus* with habitat data (Mullen et al. 2018; Shavrin 2014, 2020) only two (25%) have been collected on or near snowfields, while of the 13 large-bodied species, all have been collected on or near snowfields. The two small bodied species that have been collected in association with snow (*P. houkae* and *P. lagrandeuri*) were also the only two small-bodied species phylogenetically close to the large-bodied *P. elongatus* – sister to *P. houkae* in the concatenated analysis (Fig. 4), and sister to *P. lagrandeuri* in the COI analysis (Fig. 5). If there is some biological relationship between larger body sizes and use of snowfields as a habitat, this may also have evolved twice in the genus. However, our test of the correlation of these characters failed to reject the null hypothesis of independence and thus did not support a hypothesis of relationship between large body size and snowfield habitats. This might be due to a loss of power resulting from the tree not being fully resolved.

Phlaeopterus elongatus, the large-bodied species that did not group with the other large-bodied species, is unusual with a general habitus (Fig. 1) unlike the other large-bodied *Phlaeopterus*, resembling more an elongated small-bodied species similar to *P. lagrandeuri* or *P. houkae* – as if a small species had been "stretched." The pronotum shape of *P. elongatus*, which has deflexed lateral margins in the posterior half, is similar to the large-bodied species *P. filicornis* and *P. hatchi* (fig. 17C, D, E in Mullen et al. 2018), and Campbell placed these three species together in his '*filicornis*' species group (Tables 1, 3), but the pronotum of *P. elongatus* lacks the deeply impressed lateral foveae and we therefore consider its pronotum closer in condition to that of the small-bodied species *P. houkae* and *P. obsoletus* (fig. 15F, H in Mullen et al. 2018). Additionally, the aedeagus of *P. elongatus* is unusually small relative to its body length, with a ratio similar to that of the small-bodied species *P. obsoletus* and *P. lagrandeuri* (Fig. 7). All the large-bodied species except *P. elongatus* have wide bodies with their lengths less than 2.9 times their widths (Fig. 1), while *P. elongatus* and *P. houkae* are the only elongate species in the genus,

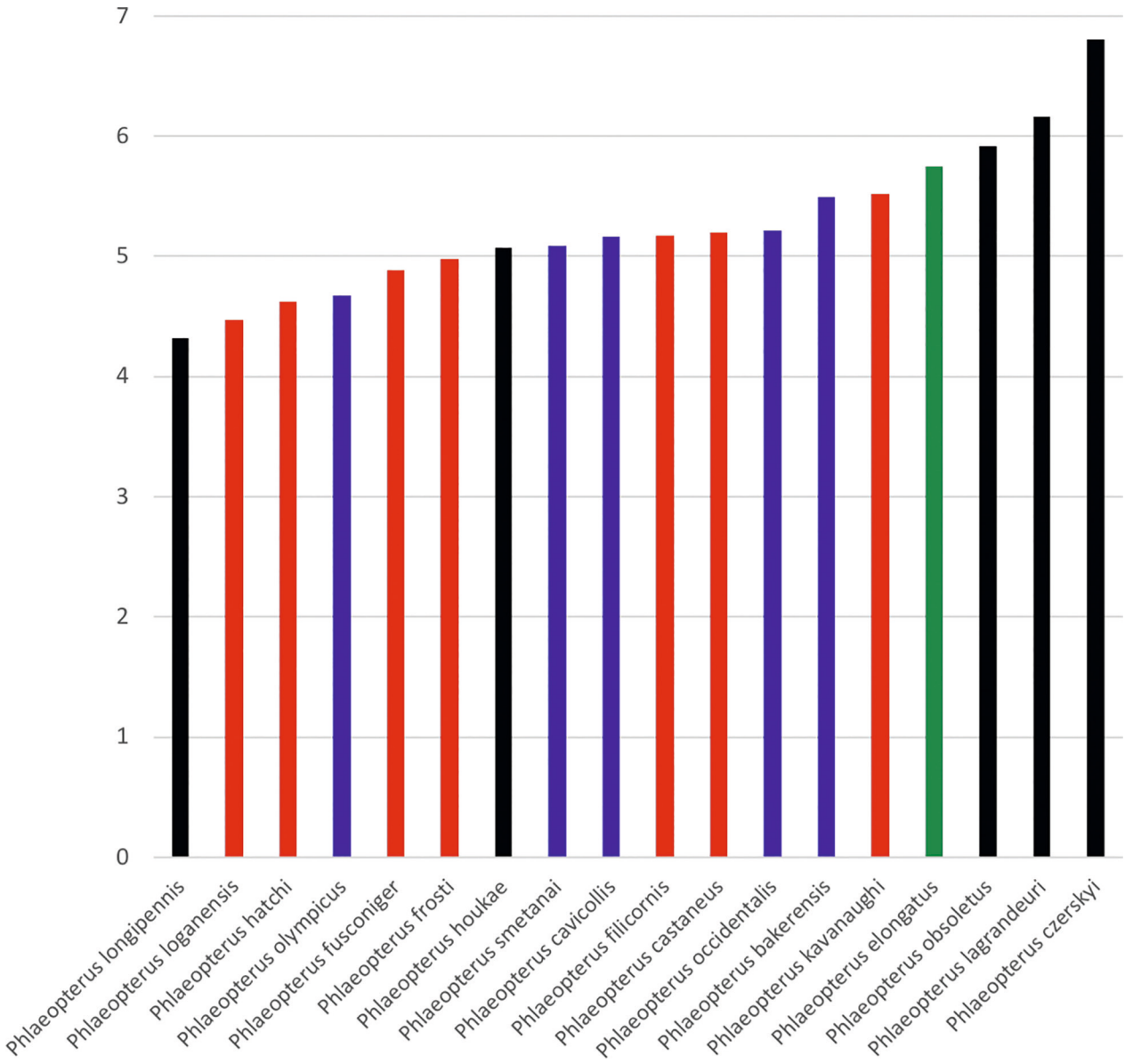

Figure 7. Body length to aedeagus length ratios for *Phlaeopterus* species sorted from smallest ratio on left (i.e. longest aedeagus relative to body length) to largest ratio on right (i.e. shortest aedeagus relative to body length). Bars in blue are species with maximum body sizes over 8 mm; bars in red are species with maximum body sizes 6.5 to 7.9 mm with wide bodies; bars in black are species with maximum body sizes below 5 mm; the green bar is for *P. elongatus* with a maximum body size of 6.4 mm, with an elongate body. Data from Mullen et al. 2018.

with their lengths 3.1 and 3.2 times their widths, respectively. There are four characters in our morphology matrix that support the monophyly of the wide, large-bodied species to the exclusion of *P. elongatus*: antocellar foveae shape (character = chr. 6), dorsal surface of labrum (chr. 11), lateral area of pronotum (chr. 22), and metathoracic wings (chr. 30).

However, there are characters that show homoplasy and leave open the question of the true ancestry of *P. elongatus*, such as the larger spicules on the internal sac of the aedeagus, chr. 39 (fig. 21A–D in Mullen et al. 2018), which are shared by four of the five small-bodied species but absent in *P. elongatus* and *P. czerskyi*, which have only small, more numerous microspicules on their internal sacs similar to all the species of large-bodied *Phlaeopterus*. The outgroup taxa have either no microspinules or very few fine microspinules on the internal sac. Additionally, the apical portion of the mesotibia (chr. 31) is glabrous in *P. elongatus* and all of the large-bodied species except the sister species pair *P. castaneus*, and *P. kavanaughi*, while it is pubescent in all the small-bodied species.

The presence of ocelli in the genus and outgroup taxa, and nearly all other taxa of Omaliinae, suggests these were present in the most recent common ancestor (proportional likelihood of 99.99%) and lost once in the ancestor of the small-bodied sister species pair of *P. obsoletus* and *P. longipennis*, but retained in the 16 other members of the genus in our study. These two species without ocelli have been found in similar or the same habitats as those with ocelli (near streams, in wet moss, in wet debris, near snow melt runoff, and near splash zones of waterfalls), so

the loss of ocelli in these species does not seem to have a relationship to their habitat preferences.

The one Palearctic species of *Phlaeopterus* in our study, *P. czerskyi*, was recovered in the basal grade as one of the five small-bodied species (Figs 4, 6), but as the sister species to the rest of *Phlaeopterus* in the morphology-only analysis (Fig. 6). These results reject a hypothesis of *P. czerskyi* being in a highly derived position within *Phlaeopterus*, and thus argue against a biogeographic hypothesis that the Palearctic *P. czerskyi* resulted from a relatively recent (within the evolutionary history of the genus) dispersal event from the Nearctic to the Palearctic. *Unamis*, which we used as an outgroup and which may be the sister genus to *Phlaeopterus*, is currently described only from the Nearctic, but it, and other omaliine genera (including other anthophagine genera) have relatively recently been found to occur in eastern Asia as well as North America, or *vice versa* (Newton et al. 2000). Thus, further study is needed, including addition of the newly documented Asian *Phlaeopterus* species and much greater outgroup and character sampling, to confidently infer the phylogeny and biogeographic origin of the genus. *Phlaeopterus czerskyi* was not found to be a sister species of, nor very similar to, any of the other *Phlaeopterus* in our study, which raises questions about the basal radiation of the genus, its generic limits, and its relationship to *Unamis* to be explored in future studies.

4.1. Conflict and agreement in analyses of morphology vs. molecules

Differences in topology, resolution, and branch support were observed between the concatenated COI+morphology (Fig. 4), COI-only (Fig. 5), and morphology-only (Fig. 6), analyses. A strict consensus tree of all three final topologies, limited to the taxa for which we have DNA data, shares only two clades within *Phlaeopterus* – a polytomous clade of the wide, large-bodied species nested within the small-bodied species and *P. elongatus* (i.e., a clade of all *Phlaeopterus* species). Using the full taxon set, comparing the topologies of the concatenated and morphology-only data, three shared sister-species clades exist: *P. hatchi* + *P. filicornis*, *P. frosti* + *P. fusconiger*, and *P. longipennis* + *P. obsoletus*. These analyses also share a clade containing all *Phlaeopterus* species. Additionally, both datasets and all three analyses place *P. castaneus* and *P. kavanaughi* as close relatives with moderate to strong support – differing only in their relationship to *P. loganensis* as described in section 4.2. below. No other groupings are shared between the COI and morphology results.

The mitochondrial genome has an effective population size that is ¼ that of the somatic portions of the nuclear genome in diploid organisms, resulting in much shorter coalescence times, which should help detect closely timed speciation events but is more likely to suffer from saturation than nuclear DNA (Wiens and Penkrot 2002). Low PP and ML bootstrap values in the backbone of the COI phylogeny (Fig. 5) suggests that saturation may be confounding the phylogenetic signal of this dataset at deeper ingroup nodes. Morphological data provides a useful contrast to mtDNA, as each morphological character is coded by potentially multiple nuclear markers, and therefore may approximate their phylogenetic signal. Each type of data has strengths and limitations, and the strengths of each can complement the limitations of others. Hillis and Wiens (2000) and Wiens (2004) provide excellent summaries of the arguments for the use of both morphological and molecular data in phylogenetic analysis. In cases of conflict between morphology (Fig. 6) and COI (Fig. 5), such as the relationship of *P. elongatus* to *P. lagrandeuri*, the concatenated phylogeny (Fig. 4) recovered a topology more similar to the morphology-only phylogeny (Fig. 6), suggesting the signal in the morphological data is stronger than that in the COI data in that instance.

4.2. Identical or highly similar COI sequences in a morphologically distinct species pair

One *Phlaeopterus* species pair forms an intermixed clade in the full COI phylogeny (Fig. 5) viz. *P. loganensis* + *P. castaneus*. In an analysis of uncorrected within- and among-species p-distances these two species have uncorrected among-species p-distances of less than 2%. Specimens of *P. castaneus* (Table 2, UAMObs:Ento:232749) and *P. loganensis* (Table 2, UAMObs:Ento:232748) have 100% identical COI haplotypes. Further investigation suggests that human error is unlikely to be the explanation for these identical sequences in these two species. The two specimens were collected from different localities and sequenced by different laboratories, and the identifications of these two specimens has been confirmed by Anthony Davies of the Canadian National Collection of Insects and the second author. Morphologically, these two species are easily distinguished with the naked eye: *P. loganensis* has the autapomorphy of the elytra being prolonged at the suture in both males and females (fig. 29E in Mullen et al. 2018) whereas *P. castaneus* has broadly rounded elytral margins typical of *Phlaeopterus* and related taxa (fig. 29F, G in Mullen et al. 2018). Furthermore, these results are corroborated by a second pair of *P. castaneus* and *P. loganensis* sequences with less than 1% divergence. The known distribution of *P. loganensis* is entirely within that of *P. castaneus*.

Interestingly, *P. castaneus* forms two distinct clades in the full COI phylogeny (marked a' and a'' in Fig. 5) each corresponding with the subspecies recognized by Mullen et al. (2018), which corresponds with the high within-species COI distances we document in this species (2.29–3.08%). Only the inland Rocky Mountain *P. castaneus castaneus* clade has intermixed *P. loganensis* COI sequences. The other clade, *P. castaneus cascadiensis* Hatch, 1957, contains only two sequences, both from coastal mountain ranges, one from Haines, Alaska, and one from Mt. Garibaldi near Vancouver, British Columbia (see fig. 6B in Mullen et al. 2018 for a distribution map

of *P. castaneus*). This pattern suggests that *P. castaneus* may have hybridized with *P. loganensis* in the Rocky Mountains (*P. loganensis* is only known from the Rocky Mountains and Selkirk Mountains, fig. 12A in Mullen et al. 2018) and that the Rocky Mountain *P. castaneus castaneus* haplotype replaced the *P. loganensis* haplotype. Or, alternatively, the *P. loganensis* haplotype replaced the *P. castaneus castaneus* haplotype. However, there is no morphological evidence suggesting these two species are closely related (Fig. 6), which suggests the two subspecies would not both join with *P. loganensis* in the COI analysis, thereby making the former hypothesis more likely. The two *P. castaneus* sequences from the coastal mountains correspond to the subspecies *P. castaneus cascadiensis* (marked a'' in Fig. 5) these two subspecies overlap in Garibaldi and Manning Provincial Parks, British Columbia. These subspecies fall into two BINs on BOLD with BOLD:ACH1347 for *P. c. cascadiensis* and BOLD:AAP7088 for *P. c. castaneus*. Further study of these subspecies, particularly in their zone of sympatry, is warranted to rigorously test their subspecies status.

These results may also be due to incomplete lineage sorting (Maddison 1997) or infections of the bacterium *Wolbachia* (Whitworth et al. 2007). Studies of sequence divergence within various insect groups have reported large variation of within- and among-species distances (Cognato 2006; Trewick 2008) and high rates of non-monophyly of animal species (Funk and Omland 2003). These issues might disappear with a larger dataset including additional mitochondrial and nuclear loci, which are less likely to be introgressed. Therefore, in this case we have based our conclusions regarding species status on the morphological phylogenetic signal.

4.3. Characters of generic relevance

Although our survey of character states in the outgroup taxa was rather cursory and relied in part on J.M. Campbell's assessments, these analyses suggest the following character states might be of value for further study of inter-generic relationships. *Phlaeopterus* and its presumed sister group, *Unamis*, share the following: the labrum has micropores (chr. 11), the minimum width of the gula is wide, more than 0.2 times as wide as the mentum (chr. 12), the center of the epipharynx has many closely spaced small spines (chr. 15), the fine cilia at the base of the hypopharynx are not in rows (chr. 17), the molar area of the mandible is without setae (chr. 19), the prosthecal fringe of the mandible extends beyond the subapical tooth (chr. 20), the lateral area of the pronotum is moderately to deeply impressed, foveiform (chr. 22), and the first metatarsomere is subequal to or longer than the ultimate metatarsomere (chr. 35). *Unamis* is autapomorphic in having a narrow labrum less than 0.3 times as long as wide (chr. 10) and the apical portion of the epipharynx is smooth and without spines (chr. 14). Additional characters diagnostic of *Unamis* are provided in Newton et al. (2000). Characters diagnostic of *Phlaeopterus* are listed in Mullen et al. (2018) and Newton et al. (2000).

4.4. Future directions for phylogenetics of the Anthophagini

The phylogeny of the tribe Anthophagini, to which *Phlaeopterus* belongs, is largely unknown. The tribe contains 27 North American genera, of which only six have been revised taxonomically (Campbell 1978, 1979, 1982, 1983, 1984; Mullen et al. 2018) and 43 genera globally (Kim et al. 2019). Furthermore, the tribe Anthophagini has been referred to as a taxonomic dumping ground, as it lacks synapomorphies and is likely not monophyletic (Newton et al. 2000; Kim et al. 2019). Kim et al. (2019) performed a phylogenetic analysis of the subfamily Omaliinae using three mitochondrial and three nuclear markers. Their analysis did not support the monophyly of the subfamily Omaliinae or the tribe Anthophagini, which formed two widely separated clades in their Bayesian analysis – one entirely of species of *Lesteva*, and the other with 11 other anthophagine genera and four coryphiine genera. No species of *Phlaeopterus* or *Unamis* were included in the taxon sampling of Kim et al. (2019). Given that a number of the deep branches in the phylogeny of Kim et al. (2019) were not strongly supported, despite their large dataset of six genetic markers, it will probably require much denser taxon sampling combined with next-generation sequencing and phylogenomic methods to confidently resolve the phylogeny of the Omaliinae.

Testing the monophyly of *Phlaeopterus* properly would also require much denser taxon sampling, including more *Lesteva* species, the addition of all or most of the known *Unamis* species, and representatives of most other anthophagine genera, in combination with a much larger genetic dataset. Although the large- and wide-bodied species form a well delimited clade, the delimitation between the remaining *Phlaeopterus*, especially the newly added Asian species, and the outgroup taxa is relatively subtle. Greater focus on inter-generic characters and relationships is warranted in future studies.

Here, we present the first phylogeny of the genus *Phlaeopterus*, and the first modern phylogenetic reconstruction of species-level relationships within the rove beetle subfamily Omaliinae using both morphology and molecular data. It is our hope that the coming years will see the production of much needed phylogenetic and taxonomic revisions of other anthophagine genera, resolving tribal, generic, and sub-generic relationships within the Omaliinae.

5. Author contributions

Derek Sikes conceived study questions and guided the research process, scored much of the final morphological data, performed analyses, contributed equipment, specimens, and other resources, and re-wrote the manuscript. Logan Mullen collected specimens, DNA data, performed preliminary analyses, and drafted the manuscript.

6. Acknowledgements

We thank Milt Campbell for sharing with us his unpublished research from the 1980s on the evolution of *Phlaeopterus*. We thank the 35 institutions and respective staff that enabled this research by providing specimen loans. We thank Patrice Bouchard and Anthony Davies of the Canadian National Collection of Insects, Arachnids, and Nematodes, Ottawa, Canada who arranged an enormous loan and helped this project in various ways. We thank Alexey Shavrin, David Kavanaugh, Vladimir Gusarov, Link Olson, Jessica Rykken, and Jim LeBonte for donating specimens to this study, and Sarah Meierotto and Jessica Rykken for assistance collecting specimens in the field. We thank Kathryn Daly, Adam Haberski, and Miles McHugh for their assistance databasing specimens and managing loans. The second author is particularly grateful to his wife, Sydney Brannoch, for her assistance throughout the research and writing process. We thank Alexey Shavrin for helpful edits of the manuscript and providing the Zanetti (2012) body size reference. We thank Margaret Thayer for her insightful comments on the morphological data and detailed critique of the manuscript. We thank Paul Lewis for explaining the importance of tree topology priors on constrained analyses and Bayes factors tests, as well as explaining how to interpret results from stepping stone sampling. We also thank two anonymous reviewers and editor Martin Fikáček for suggestions that improved the manuscript. This research was supported by funding from the Society of Systematic Biologists, the Arctic Audubon Society, a Kenelm Philip Entomology Research Award from the Alaska Entomological Society, the SysEB section of the Entomological Society of America, and the UAF Biology Graduate Student Association.

7. References

Bergsten J, Nilsson AN, Ronquist F (2013) Bayesian tests of topology hypotheses with an example from diving beetles. Systematic Biology 62(5): 660–673.

Campbell JM (1978) A revision of the North American Omaliinae (Coleoptera: Staphylinidae) 1. The genera *Haida* Keen, *Pseudohaida* Hatch, and *Eudectoides* new genus. Memoirs of the Entomological Society of Canada 110(106): 1–20.

Campbell JM (1979) A revision of the North American Omaliinae (Coleoptera: Staphylinidae): 2. The tribe Coryphiini. Memoirs of the Entomological Society of Canada 110: 21–86.

Campbell JM (1982) A revision of the North American Omaliinae (Coleoptera: Staphylinidae): 3. The genus *Acidota* Stephens. The Canadian Entomologist 114(11): 1003–1029.

Campbell JM (1983) A revision of the North American Omaliinae (Coleoptera: Staphylinidae): 4. The genus *Olophrum* Erichson. The Canadian Entomologist 115(6): 577–622.

Campbell JM (1984) A revision of the North American Omaliinae (Coleoptera: Staphylinidae): 5. The genera *Arpedium* Erichson and *Eucnecosum* Reitter. The Canadian Entomologist 11(6): 487–527.

Casey TL (1885) New genera and species of Californian Coleoptera. Bulletin of the California Academy of Sciences 7: 281–606.

Casey TL (1886) Descriptive notices of North American Coleoptera I. Bulletin of the California Academy of Sciences 2(6): 157–264.

Casey TL (1893) Coleopterological Notices V. Annals of the New York Academy of Sciences 7(1): 281–624.

Cognato AI (2006) Standard percent DNA sequence difference for insects does not predict species boundaries. Journal of Economic Entomology 99(4): 1037–1045.

Cunningham CW, Omland KE, Oakley TH (1998) Reconstructing ancestral character states: a critical reappraisal. Trends in Ecology and Evolution 13(9): 361–366.

Dowton M, Austin AD (1997) Evidence for AT-transversion bias in wasp (Hymenoptera: Symphyta) mitochondrial genes and its implications for the origin of parasitism. Journal of Molecular Evolution 44(4): 398–405.

Fauvel A (1878) Les Staphylinides de l'Amerique du Nord. Notices Entomologiques 7: 1–100.

Folmer O, Black M, Hoeh W, Lutz R, Vrijenhoek R (1994) DNA primers for amplification of mitochondrial cytochrome c oxidase subunit I from diverse metazoan invertebrates. Molecular Marine Biology and Biotechnology 3(5): 294–299.

Funk DJ, Omland KE (2003) Species-level paraphyly and polyphyly: frequency, causes, and consequences, with insights from animal mitochondrial DNA. Annual Review of Ecology, Evolution, and Systematics 34(1): 397–423.

Griekspoor A, Groothuis T (2005) 4Peaks, version 1.7. Nucleobytes.com.

Guindon S, Dufayard JF, Lefort V, Anisimova M, Hordijk W, Gascuel O (2010) New algorithms and methods to estimate maximum-likelihood phylogenies: assessing the performance of PhyML 3.0. Systematic Biology 59(3): 307–321.

Hatch MH (1957) The Beetles of the Pacific Northwest: Part II: Staphyliniformia. With the collaboration of MW Sanders and GA Marsh. University of Washington Press: Seattle, WA, USA: 16(2): i–ix + 1–384.

Hendrich L, Morinière J, Haszprunar G, Hebert PD, Hausmann A, Köhler F, Balke M (2015) A comprehensive DNA barcode database for Central European beetles with a focus on Germany: adding more than 3500 identified species to BOLD. Molecular Ecology Resources 15(4): 795–818.

Hillis DM, Wiens JJ (2000) Molecules versus morphology in systematics: conflicts, artifacts, and misconceptions. In: Phylogenetic Analysis of Morphological Data (Wiens J Ed.). Smithsonian Institution Press: Washington, DC. pp. 1–19.

Holder M, Lewis P (2003) Phylogeny estimation: traditional and Bayesian approaches. Nature Reviews Genetics 4: 275–284 doi:10.1038/nrg1044

Kass RE, Raftery AE (1995) Bayes factors. Journal of the American Statistical Association 90(430): 773–795.

Kim TK, Song JH, Thayer MK, Ahn KJ (2019) Molecular phylogeny of Omaliinae (Coleoptera: Staphylinidae) and its implications for evolution of atypically long elytra in rove beetles. Systematic Entomology 45(1): 20–32.

Lanfear R, Frandsen PB, Wright AM, Senfeld T, Calcott B (2016) PartitionFinder 2: new methods for selecting partitioned models of evolution for molecular and morphological phylogenetic analyses. Molecular Biology and Evolution 34(3): 772–773. DOI: dx.doi.org/10.1093/molbev/msw260

Lewis PO (2001) A likelihood approach to estimating phylogeny from discrete morphological character data. Systematic Biology 50(6): 913–925.

Maddison WP (1997) Gene trees in species trees. Systematic Biology 46(3): 523–536.

Maddison DR, Maddison WP (2005) MacClade 4: Analysis of phylogeny and character evolution, version 4.08 a.

Maddison WP, Maddison DR (2016) Mesquite: a modular system for evolutionary analysis, version 3.10. http://mesquiteproject.org

Miller MA, Pfeiffer W, Schwartz T (2010) Creating the CIPRES Science Gateway for inference of large phylogenetic trees. Pp. 1–8 in: 2010 Gateway Computing Environments Workshop (GCE).

Miller RE, Buckley TR, Manos PS (2002) An examination of the monophyly of morning glory taxa using Bayesian phylogenetic inference. Systematic Biology 51(5): 740–753.

Moore I, Legner EF (1979) An illustrated guide to the genera of the Staphylinidae of America North of Mexico exclusive of the Aleocharinae (Coleoptera). Division of Agricultural Sciences, University of California Priced Publication 4093. 332 pp.

Motschulsky VI (1853) Etudes Entomologiques. La Société de Litérature Finnoise, Helsinki. 192 pp.

Mullen LJ, Campbell JM, Sikes DS (2018) Taxonomic revision of the rove beetle genus *Phlaeopterus* Motschulsky, 1853 (Coleoptera: Staphylinidae: Omaliinae: Anthophagini). The Coleopterists Bulletin 72(monograph16): 1–54.

Newton AF, Thayer MK, Ashe JS, Chandler DS (2000) 22. Staphylinidae Latreille, 1802. Pp. 272–418 in: Arnett RH, Thomas MC (Eds), American Beetles, Vol. 1. Archostemata, Myxophaga, Adephaga, Polyphaga: Staphyliniformia. CRC Press.

Pagel M (1994) Detecting correlated evolution on phylogenies: a general method for the comparative analysis of discrete characters. Proceedings of the Royal Society London B 255: 37–45.

Pentinsaari M, Hebert PDN, Mutanen M (2014) Barcoding beetles: A regional survey of 1872 species reveals high identification success and unusually deep interspecific divergences. PLoS ONE 9(9): e108651.

R Core Team (2020) R: A language and environment for statistical computing. R Foundation for Statistical Computing, Vienna, Austria. URL https://www.R-project.org

RStudio Team (2020) RStudio: Integrated Development for R. RStudio, Inc., Boston, MA. URL http://www.rstudio.com

Ronquist F, Teslenko M, Van Der Mark P, Ayres DL, Darling A, Höhna S, Larget B, Liu L, Suchard MA, Huelsenbeck JP (2012) MrBayes 3.2: efficient Bayesian phylogenetic inference and model choice across a large model space. Systematic Biology 61(3): 539–542.

Ronquist F, Huelsenbeck J, Teslenko M, Zhang C, Nylander JAA (2020) MrBayes version 3.2 Manual: Tutorials and Model Summaries. https://nbisweden.github.io/MrBayes/manual.html, pp.1–152.

Rougemont G-M de (2000) New species of *Lesteva* Latreille, 1796 from China (Insecta: Coleoptera: Staphylinidae). Annalen des Naturhistorischen Museums in Wien 102 (B): 147–169.

Scheerpeltz O (1933) Staphylinidae VII. In: Coleopterorum Catalogus (Schenkling S ed.) 129: 989–1500.

Shavrin AV (2001) New and little-known species of Omaliinae from the Baikal-Transbaikal area (Coleoptera: Staphylinidae). Zoosystematica Rossica 9(1): 189–193.

Shavrin AV (2014) Two new species and records of the genus *Lesteva* Latreille, 1797 (Coleoptera: Staphylinidae: Omaliinae) from southeastern China. Zootaxa 3821(2): 291–296. https://doi.org/10.11646/zootaxa.3821.2.10

Shavrin AV (2020) The Chinese species of the genus *Phlaeopterus* Motschulsky, 1853 (Coleoptera: Staphylinidae: Omaliinae: Anthophagini). Zootaxa 4722(4): 395–400.

Shavrin AV, Mullen LJ (2015) *Phlaeopterus* Motschulsky, 1853 (Coleoptera: Staphylinidae: Omaliinae: Anthophagini) – a new genus for the Palaearctic: new combination. Zootaxa 4028(1): 121–128.

Shavrin AV, Yamamoto S (2019) Unexpected palaeodiversity of omaliine rove beetles in Eocene Baltic amber (Coleoptera, Staphylinidae, Omaliinae). ZooKeys 863: 35.

Shorthouse DP (2010) SimpleMappr, an online tool to produce publication-quality point maps. [Retrieved from http://www.simplemappr.net. Accessed 25 June 2020.]

Sikes DS, Bowser M, Morton JM, Bickford C, Meierotto S, Hildebrandt K (2017) Building a DNA barcode library of Alaska's non-marine arthropods. Genome 60(3): 248–259.

Stone G, French V (2003) Evolution: have wings come, gone and come again? Current Biology 13(11): R436–R438.

Swofford DL (2002) PAUP*. Phylogenetic Analysis Using Parsimony (*And Other Methods), version 4. Sinauer Associates, Sunderland, Massachusetts.

Thayer MK (2016) Staphylinidae Latreille, 1802. Handbook of Zoology. Coleoptera, Beetles, Volume 1: Morphology and Systematics (Archostemata, Adephaga, Myxophaga, Polyphaga partim), 2nd edn (Beutel RG and Leschen RAB Eds), pp. 394–442. Walter de Gruyter GmbH, Berlin/Boston, Massachusetts.

Trewick SA (2008) DNA Barcoding is not enough: mismatch of taxonomy and genealogy in New Zealand grasshoppers (Orthoptera: Acrididae). Cladistics 24(2): 240–254.

Whiting MF, Bradler S, Maxwell T (2003) Loss and recovery of wings in stick insects. Nature 421(6920): 264–267.

Whitworth TL, Dawson RD, Magalon H, Baudry E (2007) DNA barcoding cannot reliably identify species of the blowfly genus *Protocalliphora* (Diptera: Calliphoridae). Proceedings of the Royal Society of London B: Biological Sciences 274(1619): 1731–1739.

Wiens JJ (2004) The role of morphological data in phylogeny reconstruction. Systematic Biology 53(4): 653–61.

Wiens JJ, Penkrot TA (2002) Delimiting species using DNA and morphological variation and discordant species limits in spiny lizards (*Sceloporus*). Systematic Biology 51(1): 69–91.

Wright AM, Hillis DM (2014) Bayesian analysis using a simple likelihood model outperforms parsimony for estimation of phylogeny from discrete morphological data. PLoS One 9(10): e109210.

Zanetti A (2012) Unterfamilie Omaliinae. In: Assing V and Schülke M (Eds), Freude-Harde-Lohse-Klausnitzer, Die Käfer Mitteleuropas, Band 4: Staphylinidae I. Zweite neubearbeitete Auflage. Spektrum Akademischer Verlag, Heidelberg, pp. 49−117.

Zwickl DJ (2006) Genetic algorithm approaches for the phylogenetic analysis of large biological sequence datasets under the maximum likelihood criterion. Ph.D. dissertation, The University of Texas at Austin.

Xie W, Lewis PO, Fan Y, Kuo L, Chen MH (2011) Improving marginal likelihood estimation for Bayesian phylogenetic model selection. Systematic Biology 60(2): 150–160.

Supplementary materials

File 1

Authors: Sikes DS, Mullen LL (2021)
Data type: .nex
Explanation note: Data file used for combined phylogenetic analyses.

Link: https://doi.org/10.3897/asp.79.e62554.suppl1

File 2

Authors: Sikes DS, Mullen LL (2021)
Data type: .nex
Explanation note: Data file used for molecular phylogenetic analyses.

Link: https://doi.org/10.3897/asp.79.e62554.suppl2

File 3

Authors: Sikes DS, Mullen LL (2021)
Data type: .nex
Explanation note: Data file used for morphological phylogenetic analyses.

Link: https://doi.org/10.3897/asp.79.e62554.suppl3